



THE EFFECTS OF PRESSURE AND TEMPERATURE ON ALKALINE ELECTROLYSIS

Lappeenranta–Lahti University of Technology LUT

Chemical Engineering Master's thesis

2024

Eliezel Mukiza

Examiner(s): Docent Arto Laari

Assistant Professor Nima Rezaei

ABSTRACT

Lappeenranta–Lahti University of Technology LUT
LUT School of Engineering Sciences
Degree Programme in Chemical Engineering

Eliezel Mukiza

The effects of pressure and temperature on alkaline electrolysis

Master's thesis

2024

91 pages, 24 figures, 19 tables and 8 appendices

Examiners: Docent Arto Laari
Assistant Professor Nima Rezaei

Keywords: High temperature, Alkaline electrolysis, high pressure, electrolysis model, hydrogen production, Aspen Plus

Green hydrogen offers a sustainable energy solution that significantly lowers greenhouse gas emissions and helps reduce the consequences of climate change. Unlike fossil fuels, green hydrogen production does not emit polluting gases, aligning with global decarbonization goals. Alkaline electrolysis is crucial for the production of green hydrogen and the storage of electrical energy.

This study investigates strategies to improve the efficiency of alkaline electrolysis by optimizing operating conditions such as pressure and temperature to minimize energy consumption. By improving the electrochemical performance and reducing overvoltage potentials, significant energy savings can be achieved, making green hydrogen production more economically viable and scalable. Lower energy consumption maximizes the utilization of renewable energy sources, reducing reliance of fossil fuels and decreasing hydrogen production costs.

A system efficiency of 69-85% at a current density of 0.35 A/cm² was achieved for the simulated process, based on hydrogen high heating value, at temperatures between 60°C and 150°C. Energy consumption was 57.20 kWh/kg H₂ at 60°C and 46.49 kWh/kg H₂ at 150°C, demonstrating the significant impact of high temperature on energy consumption in alkaline electrolysis. The influence of pressure on alkaline electrolysis was also investigated by simulating the process at various pressures. The results indicated that pressure has a minimal impact on stack performance. However, its effect on gas dissolution in the circulating electrolyte solution, and hence gas mixing, is significant and could pose a major issue if not properly managed. The study showed that the process can operate up to 30 bars, which remains within the hydrogen-to-oxygen safety limit of 2%.

Economic analysis was also conducted to investigate the effect of pressure on alkaline electrolysis equipment costs. The results revealed that increasing process pressure reduces the cost of compressors, leading to lower CAPEX, OPEX, and even hydrogen production costs.

TIIVISTELMÄ

Lappeenrannan–Lahden teknillinen yliopisto LUT
LUT Insinööritieteiden tiedekunta
Kemiantekniikka

Eliezel Mukiza

Paineen ja lämpötilan vaikutukset alkaliseen elektrolyysiin

Kemiantekniikan diplomityö

2024

91 sivua, 24 kuvaa, 19 taulukkoa ja 8 liitettä

Tarkastajat: Dosentti Arto Laari

Apulaisprofessori Nima Rezaei

Avainsanat: Alkali elektrolyysi, korkea paine, korkea lämpötila, elektrolyysin malli, vedyn tuotanto, Aspen Plus

Vihreä vety tarjoaa kestäväen energiaratkaisun, joka vähentää merkittävästi kasvihuonekaasupäästöjä ja lieventää ilmastonmuutoksen vaikutuksia. Toisin kuin fossiiliset polttoaineet, vihreän vedyn tuotanto ei tuota lainkaan hiilidioksidipäästöjä, mikä tukee globaaleja hiilidioksidin vähentämistavoitteita. Alkalielektrolyysillä on tärkeää rooli vihreän vedyn tuotannossa ja sähköenergian varastoinnissa.

Tämä tutkimus tutkii strategioita alkalielektrolyysin tehokkuuden parantamiseksi keskittyen käyttöolosuhteiden, kuten lämpötilan ja paineen, optimointiin energian käytön minimoimiseksi. Parantamalla sähkökemiallista suorituskykyä ja vähentämällä ylijännitepotentiaaleja voidaan saavuttaa merkittäviä energiansäästöjä, mikä tekee vihreän vedyn tuotannosta taloudellisesti kannattavampaa ja skaalautuvampaa. Pienempi energiankulutus ei ainoastaan vähennä vedyn tuotannon kokonaiskustannuksia, vaan myös maksimoi uusiutuvien energialähteiden hyödyntämisen ja vähentää siten riippuvuutta fossiilisista polttoaineista.

Simuloidussa prosessissa saavutettiin 69–85 % systeemihiötysuhde 0,35 A/cm² virrantiheydellä, perustuen vedyn korkeaan lämpöarvoon, lämpötiloissa 60°C ja 150°C välillä. Energiankulutus oli 57,20 kWh/kg H₂ 60°C lämpötilassa ja 46,49 kWh/kg H₂ 150°C lämpötilassa, mikä osoittaa korkean lämpötilan merkittävän vaikutuksen energiankulutukseen alkalisisessa elektrolyysissä. Paineen vaikutusta alkalielektrolyysiin tutkittiin myös simuloimalla prosessia eri paineilla. Tulokset osoittivat, että paineella on vain vähäinen vaikutus kennojen suorituskykyyn, mutta sen vaikutus kaasujen liukoisuuteen kiertävään elektrolyyttiliuokseen ja sitten kaasujen sekoittumiseen on merkittävä ja voi aiheuttaa suuria ongelmia, ellei sitä hallita kunnolla. Tutkimuksessa havaittiin, että prosessi voi toimia jopa 30 baarin paineessa, mikä pysyy vety-happi-turvarajan (2 %) sisällä.

Lisäksi tehtiin taloudellinen analyysi, jossa tutkittiin paineen vaikutusta alkalielektrolyysilaitteiden kustannuksiin. Tulokset osoittivat, että prosessipaineen lisääminen vähentää kompressorien kustannuksia, mikä johtaa alhaisempiin investointikustannuksiin, käyttökustannuksiin, ja jopa vedyn tuotantokustannuksiin.

ACKNOWLEDGEMENTS

This master's thesis was carried out at Lappeenranta-Lahti University of Technology LUT in Lappeenranta.

I would like to extend my heartfelt thanks to Docent Arto Laari for his valuable input and guidance throughout this thesis project. His assistance was invaluable, especially when things became more complicated, ensuring I fully understood my tasks. I am also grateful to Nima Rezaei and Hung Nguyen for their support.

A special thank you goes to my friends in Lappeenranta, with whom I have shared many memorable moments, both good and bad, over the years. We faced numerous group projects that seemed daunting, yet we always managed to pull through by doing what needed to be done.

Last but not least, I want to express my deepest gratitude to my family and friends for their unwavering support during my thesis and throughout my studies.

SYMBOLS AND ABBREVIATIONS

Symbols

E	voltage	V
F	Faraday constant	s A/mol
G	Gibbs free energy	kJ/mol
H	enthalpy	kJ/mol
I	current	A
p	pressure	bar, Pa
q_m	mass flow rate	kg/s
R	gas constant	J/kg K
T	temperature	°C, K
V	volume	m ³

Subscripts

a	anode
act	activation
c	cathode
con	concentration
d	diffusion
H ₂	hydrogen
H ₂ O	water
O ₂	oxygen
ohm	ohmic
rev	reversible
tn	thermoneutral

Abbreviations

AEL	Alkaline electrolysis
AEM	Anion exchange membrane
BoP	Balance of plant
CAPEX	Capital expenditure
DC	Direct current
HER	Hydrogen evolution reaction
HTO	Hydrogen in oxygen
HHV	High heating value
IRENA	International renewable energy agency
KOH	Potassium hydroxide
LHV	Low heating value
NaOH	Sodium hydroxide
OER	Oxygen evolution reaction
OTH	Oxygen in hydrogen
OPEX	Operating expenditure
P2X	Power-to-X
PEM	Proton exchange membrane
SOEC	Solid oxide electrolyzer cell

Table of Contents

SYMBOLS AND ABBREVIATIONS.....	5
1 Introduction	9
1.1 Objectives.....	10
2 Water electrolysis	11
2.1 Water electrolysis technologies.....	11
3 Alkaline electrolysis process	15
3.1 Basic principle of conventional industrial alkaline electrolysis.....	15
3.2 Materials of conventional alkaline eletrolyzer	22
3.3 Thermodynamics of water splitting	23
3.4 Electrochemistry of water splitting	27
3.5 Gas solubility	31
3.6 Alkaline electrolysis efficiency	33
4 High-pressure and high-temperature alkaline electrolysis	35
4.1 Structure of alkaline electrolysis cell at elevated temperature and pressure.....	36
4.2 Construction materials and corrosion stability.....	38
5 Cost of alkaline electrolysis	41
5.1 Cost structure of alkaline electrolysis	42
5.2 Economic analysis for conventional alkaline electrolysis	48
5.3 High pressure and high temperature influence on cost of AEL.....	51
6 Simulation	54
6.1 Objectives.....	54
6.2 Development of alkaline electrolysis process model	54
6.3 Energy and mass balance	59
6.4 Equipment sizing.....	61
6.4.1 Separation unit	61
6.4.2 DEOXO unit	62
7 Results	64
7.1 Pressure and temperature influence on AEL system.....	64
7.1.1 Temperature influence on stack performance.....	65
7.1.2 Pressure influence on stack performance.....	70
7.2 Development of electrolysis cost model	74
7.2.1 Estimation of investment capital cost	74

7.2.2	Variable costs and revenue	81
8	Conclusions	83
9	References	85
	Appendices	92

1 Introduction

Power-to-X (P2X) technology is a transformative approach in the renewable energy sector, addressing the intermittent nature of renewable energy sources and enabling to store and use excess electricity. This innovative process involves converting electrical energy, primarily from renewable energy into gaseous fuels. The demand for emission-free electrical energy is already enormous and is rapidly increasing globally. P2X mainly focuses on generating hydrogen by water electrolysis. The hydrogen produced through water electrolysis process has diverse applications: it can be used in fuel cells to generate electricity, utilized in industrial processes as raw material, or adopted as a fuel for transportation.

Currently, alkaline electrolysis (AEL) is the most developed electrolysis technology, known for its reliability and efficiency proven over decades. However, further cost reductions and efficiency improvements are necessary to make it commercially attractive. Conventional AEL, which operates at ambient temperatures and pressures, faces limitations in efficiency and productivity that hinder its widespread adoption in the rapidly evolving energy landscape. Some of the most promising modifications to the process involve raising the operating pressure and temperature of the electrolysis cells. Hu et al. (2022) found that increasing pressure can reduce investment costs by lowering the cost of hydrogen compressors. Additionally, operating at higher temperatures has been shown to enhance AEL efficiency. These advancements could significantly improve the commercial viability of AEL by addressing its current limitations.

This research aims to bridge the knowledge gap by examining the dependencies of pressure and temperature on the alkaline electrolyzer system and understanding their impact on AEL performance. Specifically, this work focuses on developing an Aspen Plus model for alkaline electrolysis that can simultaneously reduce electrolysis costs through high-pressure operation and enhance energy efficiency by enabling high-temperature conditions.

1.1 Objectives

The objective of this project is to create a process and cost model for alkaline electrolysis that can be used to assess the impact of pressure and high temperature on electrolysis efficiency. The goal is to conduct an economic analysis on alkaline electrolysis at elevated pressure and temperature, focusing on system efficiency and process costs. This project has specific objectives to answer key questions, such as:

- How do pressure and temperature influence process efficiency?
- Is there a maximum pressure level that can be used without excessive gas mixing and not overpassing the LEL limits?
- How do pressure and temperature affect capital expenditure (CAPEX) and operating expenditure (OPEX) costs?
- Are there optimal pressure and temperature levels that can reduce hydrogen costs?

The literature review will discuss water electrolysis in general and examine the current state of alkaline electrolysis, including the thermodynamics and electrochemistry associated with the process. It will also explore how existing literature has demonstrated alkaline water electrolysis at elevated pressure and temperature. The review will also touch on the status and prospects of high-temperature alkaline electrolysis, including the selection and stability of material, catalysts, and diaphragm.

2 Water electrolysis

Electrolysis, a discipline within electrochemistry, explores oxidation-reduction reactions that can transpire spontaneously or under controlled conditions. In electrolysis, these electrochemical reactions are induced by an electric current. The process involves utilizing electricity to decompose water into oxygen and hydrogen. Pure water, being a poor conductor of electricity, necessitates transformation into an electrolyte by dissolving strong acids, bases, molten salt, or other ionically soluble substances. When electrodes are linked to a battery or DC power supply, an electric current flows through the electrolyte (Tuomivirta, 2023). Cathodes and anodes within the electrolysis solution facilitate the transport of electricity. When an electric potential is applied across the electrolyte, hydrogen ions (cations), carrying a positive charge, migrate towards the negative pole (cathode), whereas hydroxide ions (anions), with a negative charge, move towards the positive pole (anode). Oxidation occurs at the anode of the electrolysis cell, while negative ions travel to the anode. During this process, hydrogen ions are reduced at the cathode to produce hydrogen gas, while hydroxide ions undergo oxidation at the anode, leading to the formation of oxygen gas. The enthalpy change associated with the decomposition of water in this reaction is 286 kJ/mol. Despite the ecological nature of electrolysis, with no greenhouse gas emissions, it demands a substantial amount of energy (Rajala, 2022).

2.1 Water electrolysis technologies

Electrolysis techniques can be broadly categorized into four main types: Alkaline electrolysis (AEL), Proton exchange membrane (PEM), Solid oxide electrolyzer cell (SOEC), and Anion exchange membrane (AEM). Apart from these, additional technologies are currently in the developmental stages, including plasma arc decomposition and photo-electrolysis (KEMI, 2022). While the operational principle remains consistent across these water electrolysis methods, the materials used, and operating conditions exhibit variations.

In Alkaline Electrolysis (AEL), the process involves immersing two metal electrodes in an alkaline solution, typically sodium hydroxide (NaOH) or potassium hydroxide (KOH). The concentration of the alkaline solution typically ranges between 20% and 40%. Nickel

commonly serves as the material for the metal electrodes. Alkaline Electrolysis (AEL) offer benefits such as inexpensive cell materials, lower investment costs, operational large-scale installations, and the absence of a need for raw water purification. However, it comes with disadvantages like requiring additional hydrogen purification, substantial space requirements for equipment, and a low current density (KEMI, 2022). A more in-depth discussion on Alkaline Electrolysis will be presented in Chapter 3.

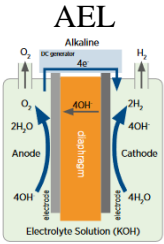
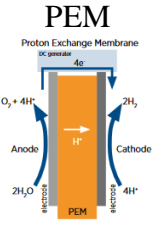
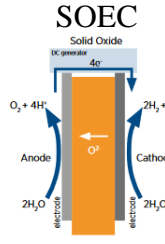
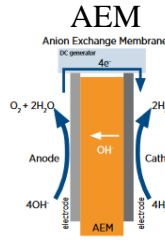
Proton exchange membrane (PEM) is one of the most popular techniques to convert renewable energy into high quality, clean hydrogen. PEM has many good features, such as high efficiency, compact system size, and high current density. In polymer electrolysis, the electrolyte is a solid polymer film. Hydrogen ions move through the polymer separator and electrons along an external route to the cathode, where combine to form a hydrogen gas. On either side of the membrane, catalysts are positioned, with the electrodes pressed against them. Due to the conduction of hydrogen ions (protons) inside the polymer membrane, the membrane surface carries a highly acidic nature. Consequently, the catalysts must be composed of noble metals to prevent corrosion from occurring (Rajala, 2022). Proton Exchange Membrane (PEM) offers benefits including flexible operation, short start-up time, the production of clean and high-pressure gas, compact spatial requirements, and the absence of the need for an electrolyte. However, it does have its drawbacks, with one significant hurdle being the necessity for IrO₂ as a catalyst. IrO₂ is not only exceedingly rare but also expensive. Consequently, the practicality of scaling up production to meet large-scale demands becomes virtually unattainable.

Solid Oxide Electrolysis Cell (SOEC) stands out as the most advanced among high-temperature electrolysis techniques. These cells demand elevated temperatures, reaching up to 1000°C, leading to superior efficiency when compared to alkaline and PEM electrolysis cells. In SOEC, water is broken down into hydrogen and oxygen by using external thermal energy and electricity. Typically constructed from stainless steel, the SOEC cell utilizes solid ceramic as both the electrolyte and membrane materials. This ceramic material excels in conducting oxygen ions at high temperatures while effectively preventing the passage of gases such as oxygen and hydrogen (Leveälähti, 2023). Solid Oxide Electrolysis Cell (SOEC) demonstrates advantages such as efficient materials (Y₂O₃, ZrO₂), enhanced energy efficiency due to high temperatures, independence from a steady electricity supply, and its applicability as a fuel cell. However, it faces challenges including the requirement for very

clean water, exceptionally high investment and operating costs, and its recent commercialization (KEMI, 2022).

Anion exchange membrane (AEM) is relatively recent technology compared to other water electrolysis and it is still in early-stage development (Faid & Sunde, 2022). AEM electrolysis is an attempt to compound the advantages of AEL and PEM electrolysis. This means that no separate electrolyte and no expensive catalyst is needed. As table 1 shows, the reactions occurring inside AEM flow cell are the same as those occurring inside an AEL flow cell (Parth, 2021). Anion Exchange Membrane (AEM) presents advantages such as high gas purity, low cost, the absence of a caustic corrosive electrolyte, cost-effectiveness without requiring costly components, and operation under high pressure. On the downside, it is still in the laboratory stage, involves excessive catalyst loading, limited durability, and faces challenges related to membrane degradation (Vincent & Bessarabov, 2017). Table 1 provides a comprehensive list of key performance indicators for the four electrolysis technologies under consideration.

Table 1. Operating principles of water electrolysis technologies (La Camera, 2020)

Specifications	AEL 	PEM 	SOEC 	AEM 
Anode reaction	$2\text{OH} \leftrightarrow \text{H}_2\text{O} + \frac{1}{2}\text{O}_2 + 2\text{e}^-$	$\text{H}_2\text{O} \leftrightarrow \frac{1}{2}\text{O}_2 + 2\text{H}^+ + 2\text{e}^-$	$\text{O}^{2-} \leftrightarrow \frac{1}{2}\text{O}_2 + 2\text{e}^-$	$2\text{OH}^- \leftrightarrow \text{H}_2\text{O} + \frac{1}{2}\text{O}_2 + 2\text{e}^-$
Cathode reaction	$2\text{H}_2\text{O} + 2\text{e}^- \leftrightarrow \text{H}_2 + 2\text{OH}^-$	$2\text{H}^+ + 2\text{e}^- \leftrightarrow \text{H}_2$	$\text{H}_2\text{O} + 2\text{e}^- \leftrightarrow \text{H}_2 + \text{O}^{2-}$	$2\text{H}_2\text{O} + 2\text{e}^- \leftrightarrow \text{H}_2 + 2\text{OH}^-$
Nominal current density (A/m ²)	2000-8000	10000-20000	3000-10000	2000-20000
Cell pressure (kPa)	< 3000	< 3000	100	< 3500
Voltage (V)	1.4-3	1.4-2.5	1.0-1.5	1.4-2.0
H ₂ purity (%)	> 99.9	> 99.9	99.9	> 99.9
Temperature (K)	343-363	323-353	973-1273	313-333
Voltage efficiency (LHV, %)	50%-68	50%-68	75%-85	52%-67
Stack electrical efficiency (kWh/kg H ₂)	47-66	47-66	35-50	51.5-66
Lifetime if stack (h)	60 000	50 000-80 000	< 20 000	> 5 000
Stack unit size (MW)	1	1	0.005	0.0025
Electrode area (m ²)	1-3	0.15	0.02	< 0.03
System electrical efficiency (MWh/t H ₂)	50-78	50-83	40-50	57-69
Stack capital cost min. 1MW (\$/kW)	270	400	> 2 000	N/A
System capital costs min. 10 MW (\$/kW)	500-1 000	700-1400	N/A	N/A

3 Alkaline electrolysis process

Alkaline electrolysis is the most advanced, developed, and well-established water electrolysis technology. It is implemented for industrial hydrogen production for many years. Although the technology is well known, progress is needed to reduce costs, improve efficiency and lifetime (Pyry, 2021). Alkaline electrolyzers operate at scales up to multi-megawatt scale and produce the cheapest hydrogen due to its lower CAPEX, maintenance, and manufacturing cost compared to other water electrolysis, however it consumes more power, leading to increased electricity costs (Nami et al., 2022). Investment costs depend largely on the production capacity of the equipment to be purchased. Alkaline electrolysis plants generally operate relatively efficiently, with efficiencies ranging from 47 % to 82 %. These efficiencies have been calculated using an upper calorific value, which assumes that the reaction products have cooled back to their initial temperature. (Viinanen, 2023).

Today, the investment costs of big units are nearly directly related to the surface area of the cell. Some companies have been manufacturing high-capacity units for advanced alkaline electrolyzers that can produce 500 to 760 Nm³/h of hydrogen, with electricity consumption of 2 MW to 5 MW (Koponen, 2015). In practice, hydrogen production can vary between 25 – 100 % of normal values, since at low current density, the mixing of gases increases in proportion to their production, leading to the formation of flammable gas mixtures. The operating pressure can vary from atmospheric pressure up to more than 400 bar, but in most cases the maximum pressure is at most in the order of 25-30 bar (Viinanen, 2023).

Hydrogen and oxygen purity levels exceed 99.5 % by volume without the need for additional purification equipment. To protect the electrodes and ensure safe operation, the equipment must be supplied with deionized water with a conductivity of less than 5 μ S/cm (Viinanen, 2023).

3.1 Basic principle of conventional industrial alkaline electrolysis

The fundamental structure of an alkaline electrolyzer is remarkably straightforward for an electrochemical system. The cell used in alkaline electrolysis usually contains two electrodes separated by a gas-impermeable porous separator, all impregnated in a liquid electrolyte.

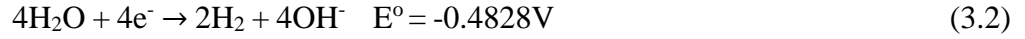
The most common electrolyte is a concentrated aqueous solution of potassium hydroxide (KOH) (usually 25-40 wt%) (Marian et al., 2022). High concentration potassium hydroxide is used to maximize ionic conductivity with KOH having a special conductivity of 0.184 S/cm. The main weakness in the use of alkaline electrolytes is that they cause corrosion inside the cell. In addition, alkaline electrolytes form a solid carbonate when they react with carbon dioxide in the air especially sodium hydroxide (NaOH) (Lahtinen, 2019). The carbonate reduces the electrical conductivity of the solution and can also cause blockages in the electrolyte circuit (Viinanen, 2023). This particular reason underscores why KOH emerge as a better choice than NaOH. The conventional alkaline electrolyzers that are commercially available today operate at temperature between 60-100°C and pressure below 30 bar. They operate at current density of 0.2-0.5 A cm⁻² with a system efficiency of 47-82% (Li et al., 2022).

The development of gaseous products from electrodes is critical because it can cause significant overvoltage, leading to a reduction in electrolysis efficiency. Electrodes must be designed to have as much contact surface with the electrolyte as possible to promote reactions. Thus, the porous structure of the electrodes is a crucial component of the process. The movement of the electrolyte solution has many beneficial effects, such as mixing, gas evolution, and heat transfer (Ursua et al., 2012).

In the process of electrolysis, an external power source such as a battery or direct current (DC) generates an electric field between the electrodes. When the DC power or battery is activated between the anode and cathode, electrons flow from the negative pole of the power source to the cathode. At the cathode, water molecules undergo decomposition, yielding hydroxide ions (OH⁻) and hydrogen gas (H₂). To preserve charge equilibrium, the hydroxide ions move across the membrane via an electric current to the anode, where they merge to generate oxygen gas (O₂) and water (H₂O) on the surface of the anode. Simultaneously, electrons (e⁻) are released, forming a closed circuit (Viinanen, 2023). Figure 1 illustrates the principle of alkaline electrolysis. The chemical reactions appearing at the anode and cathode in alkaline electrolysis are detailed below. At the anode, the following reaction occurs, where hydroxide ions oxidize to generate oxygen gas and water.



At cathode, water undergoes reduction to generate hydrogen gas and hydroxide ions (Marian et al., 2022).



Under normal conditions (at 25 °C and 1 bar), water is in liquid form and the reaction products are gases respectively, giving the total reaction of electrolysis as following.

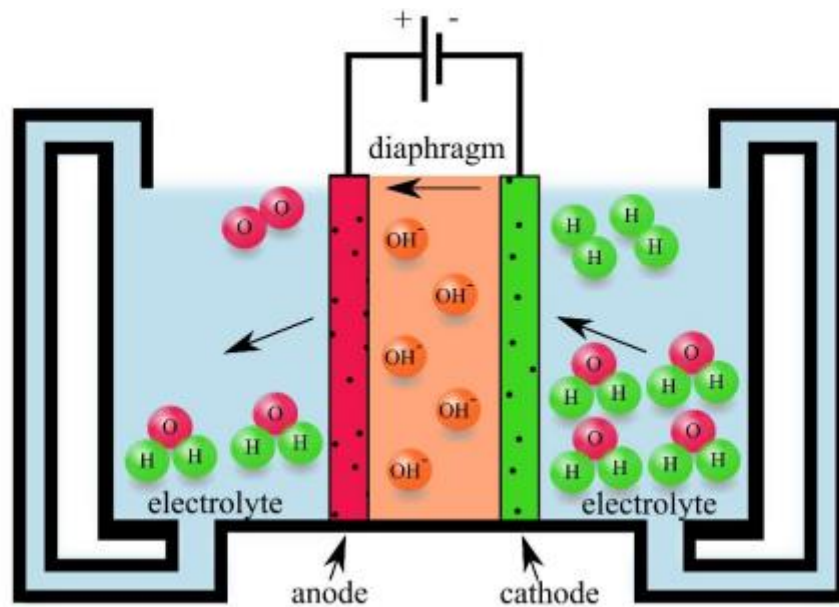


Figure 1 Fundamental layout of an alkaline electrolysis cell (Koponen, 2015)

The quantity of electrolyte solution within the electrolysis cell is determined by the distance separating the anode and the cathode. The space between the electrodes in a conventional cell design can be several centimeters. To reduce electrical losses in electrochemical cell, zero-gap has been introduced. In zero-gap design, the liquid channels are located outside the electrode with only a thin membrane separating anode and cathode. In a zero-gap configuration, the electrodes are compressed against the diaphragm (Brauns & Turek, 2020).

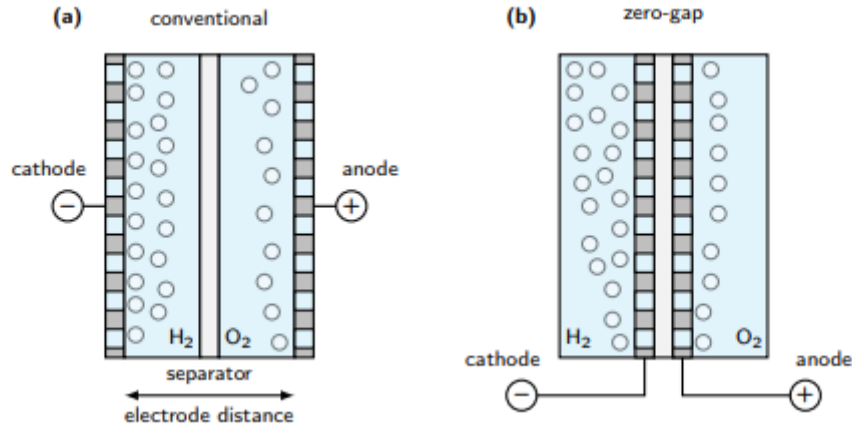


Figure 2. Conventional and zero-gap alkaline electrolyzer (Brauns & Turek, 2020)

The major difference between conventional and zero-gap design lies in the utilization of porous electrodes instead of solid metal plates. In zero-gap cell, gas bubbles are compelled to discharge from the rear of the electrodes as it shown in Fig. 2b. This phenomenon reduces gas bubbles contribution to the cell voltage, resulting in higher efficiency than in conventional electrolyzer (Phillips, 2019). In contrast to conventional cells, which employ membranes thicker than 2 mm, zero-gap cells feature membranes thinner than 0.5 mm. Zero-gap cells utilize highly porous electrodes with significant surface areas, resulting in reduced resistance to ionic transport and enhancing efficiency. The ohmic losses of the electrolyte increases with increasing distance and in fact, zero-gap diminishes ohmic resistance enabling operation with electrolytes of lower concentration. Additionally, zero-gap reduces specific power consumption. However, in small volume, the concentration of the reactive substances varies rapidly during operation (Záchenská et al., 2022). The downside of a zero-gap cell lies in the fact that as the distance between electrodes decreases, the diffusion rate of contaminant gases from one side to another increases. This leads to higher Faraday losses and a higher chances of product gas contamination (Lettenmeier, 2021).

Conventional alkaline electrolyzers use two principal configurations. The cell stack can be either unipolar or bipolar. Most manufacturers build bipolar modules, but in some special cases unipolar cells are also used. The unipolar assembly composed of alternative negative and positive electrodes separated by porous diaphragm and are suspended in a tank filled with alkaline electrolyte (Viinanen, 2023). Every electrode is directly linked to the direct power supply, so the configuration gives several individual cells in parallel (Phillips, 2019).

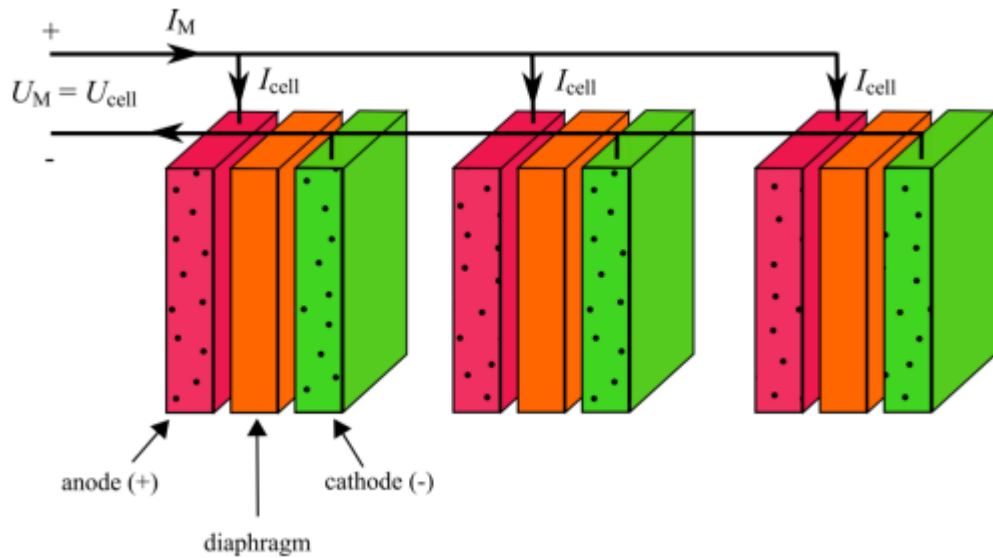


Figure 3. Monopolar cell configuration (Koponen, 2015)

The voltage of the whole unipolar electrolyzer is equivalent to the voltage between each pair of electrodes. The sum of the cell currents in unipolar configuration is equal to the total cell current I_M as it can be seen in fig. 3. In unipolar cell, each electrode undergoes either an oxidation or reduction reaction (Koponen, 2015).

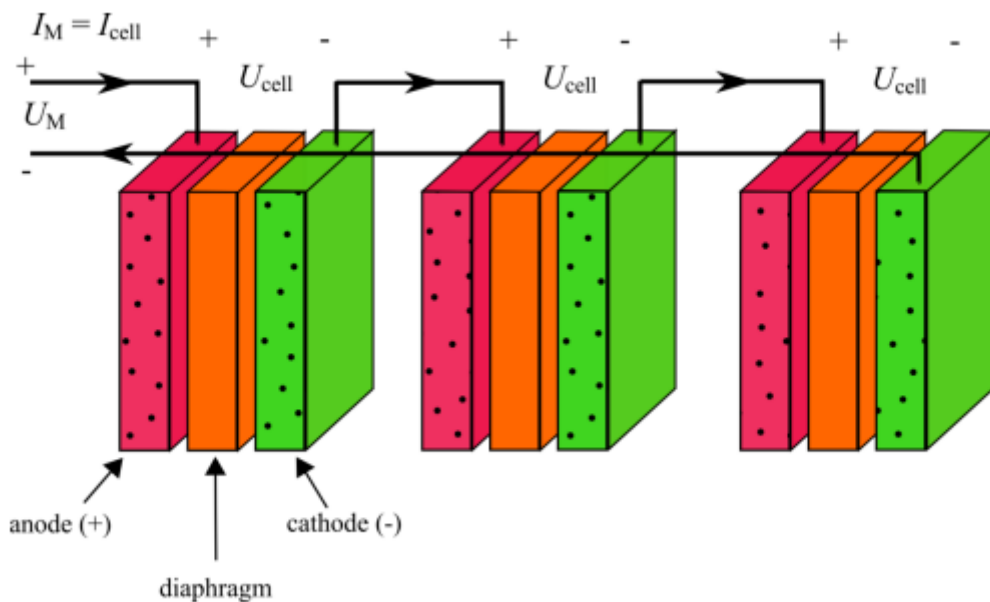


Figure 4. Bipolar cell configuration (Koponen, 2015)

In a bipolar configuration, only the two outermost electrodes are linked to the direct current power supply. This results in a series of unit cells, where current polarize each individual

electrode by flowing through the electrolyte. This polarization leads to two different reaction (oxidation & reduction) taking place at the same time on the opposite sides of each electrode (cathode and anode). Both electrode sides are used either as cathode or anode in bipolar configuration and there are not directly connect to the direct current power, except the two ends electrodes. The overall cell voltage equal to the combined voltages of each unit cells (Phillips, 2019).

Table 2. Benefits and drawbacks of unipolar and bipolar configuration (Phillips, 2019)

	Advantages	Disadvantages
Unipolar	Simple design and easy to maintain	Low voltages with high current densities
	No parasitic currents in system	Poorly suited to higher pressure
	No pump or filters required	Larger number of electrical contacts/wires
	Simple internal gas lift circulation	Deposits of corrosion and sludge products build up inside cell
Bipolar	High voltage with lower electrical current	Complex design
	More homogeneous current feeding	External pumping and filtration required
	Fewer spare parts required	Fixing a single unit cell necessitates dismantling the entire electrolyzer
	Can operate at higher pressure and temperature	Possible electrolyte leakage dangerous due to caustic electrolyte

Figure 5 illustrate the simplified conventional alkaline electrolysis. The system is fed with feed water and KOH electrolyte. Feed water and electrolyte are first purified from impurities in a purifier. The conductivity of the purified water should be below 5 $\mu\text{S}/\text{cm}$ to keep the

electrodes protected and the process safe (Lahtinen, 2019). After purification, purified water is mixed with the electrolyte. The water flows both into the electrolyte tank and into the hydrogen side separator, where it forms the concentration with the potassium hydroxide solution. The solution is fed into the system either using circulating pumps, or by gravity (La Camera, 2020). The movement of the solution provides a smoothing of the concentrations of the solution and improve heat transfer from the electrolyte. The solution progresses to the electrodes by passing across the bipolar plates and the permeable transport layers. Upon reaching the electrode, water undergoes electrolysis, dividing into oxygen and hydrogen, while ions (usually H^+ or OH^-) cross through a liquid electrolyte. The electrolysis cathode side of the electrolyzer consumes water, and the anode side produces it, so as a result, the anolyte is diluted and the catholyte is correspondingly concentrated. To compensate for the differences in concentration, the electrolytes must be mixed after gas separation as it can be seen from figure 5 below to prevent a respective dilution (Buttler & Spliethoff, 2017). The separator between the electrodes serves to keep the generated gases apart, preventing their mixing. This fundamental concept has endured for centuries, although technological advancements have progressed since its initial development by Nicholson and Anthony Carlisle in 1800 (La Camera, 2020).

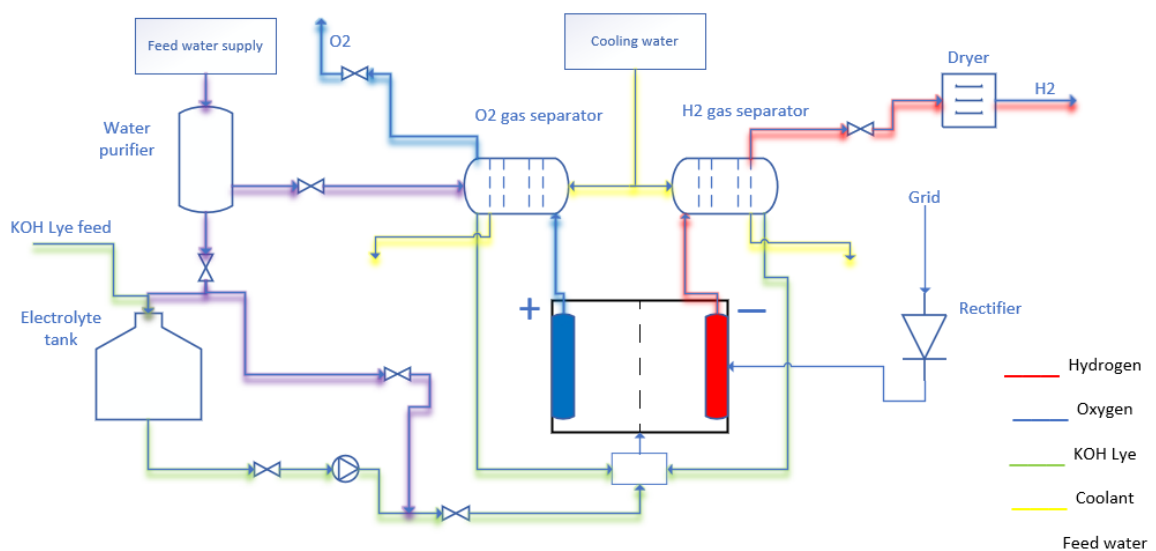


Figure 5. A simplified layout of a conventional AEL system (modified from (Buttler & Spliethoff, 2017))

Hydrogen and oxygen gas bubble flow to their separators, where they can be collected for further treatment. Some of the gases are carried with electrolyte solution to the separation, for this reason, the solution flow must be controlled to avoid a potential flammable gas mixture (Lahtinen, 2019). The separation of large gas bubbles is relatively simple as they rise to the surface of the electrolyte. However, small bubbles remain longer in solution, which makes it challenging to separate them. The typical operating temperature of a conventional electrolyzer is between 60 – 100 °C, so the gas produced, and the electrolysis mixture are cooled in the separators. The most common type of gas-liquid separator is a horizontally mounted tubular tank, where half of the tank's total volume is covered by electrolyte, and the separated gas rises to the top of the tank. The gas separator also serves as a temporary electrolyte storage. The volume of the separators must be sufficient to allow sufficient time for the electrolyte to separate small bubbles of gas (Viinanen, 2023). Once hydrogen gas is separated from the electrolyte, it is dried and then refined to the preferred level. The quality of the hydrogen gas after drying usually ranges from 99.5% to 99.9%, while the quality of the oxygen gas falls between 99% and 99.8% (Buttler & Spliethoff, 2017).

3.2 Materials of conventional alkaline electrolyzer

One of the key advantages of alkaline electrolysis over alternative techniques lies in its utilization of high pH solutions as electrolytes, eliminating the need for costly precious metal materials. This enables the use of readily available and economical electrode materials such as iron and nickel-based alloys (Viinanen, 2023). Today, nickel stands out as one of the best electrode materials thanks to its impressive corrosion resistance, high electrochemical activity, and affordability. Basic nickel electrodes have demonstrated remarkable durability in practical operations, though corrosion rates may rise when the equipment is not in use. Nickel electrodes typically exhibit an oxidation reaction overvoltage in the range of several hundred millivolts. To enhance performance, steel or nickel plates serving as electrodes are frequently coated with a nickel-iron alloy or a porous layer of nickel.

Electrocatalysts play a crucial role in water electrolysis, as their primary task is to lower the electrode voltages, thereby directly influencing electrical efficiency. This functionality significantly enhances the efficiency of the AEL process by redirecting reaction pathways

to those with lower activation energies. The advantages of elevated temperatures and the kinetics of both the oxygen evolution reaction (OER) and hydrogen evolution reaction (HER) heavily rely on the activation energy of the reaction and therefore the catalyst. (Rashid et al., 2015). Different catalysts, including metals and nickel-, iron-, cobalt-based oxides, have been employed in conventional AEL. It has been observed that combining nickel with iron, cobalt, molybdenum, chromium, and manganese enhances electrode performance, with iron exhibiting the greatest catalytic activity for OER. As for HER, the most active materials are the platinum group metals. Noble metals have been shown to possess the best catalytic activity for HER according to (Đurovič et al., 2021), but their price and shortage render them unsuitable for larger industrial applications. Several challenges remain to be addressed, particularly the OER, which is the major obstacle in the AEL process because of its inadequate stability, slow kinetics, and ohmic losses caused by bubble detachment from some catalysts (Koj et al., 2019). Compared to HER, it has been demonstrated that the overpotential of OER is immensely higher (Allebrod et al., 2012).

Polymers are commonly utilized as seals or gaskets for connections and valves, and they serve as protective layer for various components. Additionally, they are viewed as a structural material for AEL at lower temperatures (Lohmann-Richters et al., 2021). While Teflon polymer is stable and renowned for its strong alkali resistance, its high cost has compelled researchers to explore more cost-effective alternatives (Yde et al., 2013).

3.3 Thermodynamics of water splitting

The thermodynamics of electrolysis describes the equilibrium of reactions and thermal impacts within electrolysis cell. Under standard conditions of pressure and temperature (1 bar, 298 K), liquid water can be broken down into oxygen and hydrogen gases (Koponen, 2015). The process that happens in electrolysis can be described according to the fundamentals of thermodynamics (Ursua et al., 2012). The following equation express water splitting reaction:



The energy necessary to break down 1 mole of H₂O into H₂ and O₂ equals the enthalpy of formation of 1 mole of H₂O. For this reaction (3.4) to happen, part of the energy must be

electric (Gibbs free energy), and while the rest comes from the thermal energy associated with thermodynamic temperature and entropy change. The minimum quantity of energy (enthalpy) needed to decompose H₂O into H₂ and O₂ is equal to the minimum energy required (Gibbs free energy) plus thermodynamic temperature times entropy of the reaction. The enthalpy change can be represented by Eq. 3.5 (Koponen, 2015).

$$\Delta H = \Delta G + T\Delta S = -zF (E_{\text{rev}} - [T (\frac{\partial E_{\text{rev}}}{\partial T})_p]) \quad (3.5)$$

where,

z	number of moles of electrons
ΔG	Gibbs free energy change (kJ/mol)
T	thermodynamic temperature (K)
ΔS	entropy change (J/K)
F	Faraday constant
E_{rev}	the reversible voltage (V)
p	pressure (Pa)

The change in entropy ($\Delta S^\circ = + 163.15 \text{ J/ mol K}$) and enthalpy ($\Delta H^\circ = + 285.840 \text{ kJ/ mol}$) for water reaction are known, therefore Gibbs free energy is represented as following:

$$\begin{aligned} \Delta G &= \Delta H - T\Delta S & (3.6) \\ &= 285.840 \frac{\text{kJ}}{\text{mol}} - 273 \text{ K} * 163.15 \frac{\text{J}}{\text{mol K}} = 237.22 \frac{\text{kJ}}{\text{mol}} \end{aligned}$$

The electrolysis process is categorized as endothermic due to its positive enthalpy change. Additionally, ΔG is positive, indicating a nonspontaneous reaction. This underscores the necessity for an external energy source for water decomposition. Under steady temperature and pressure, the alteration in free energy aligns with the electrical work executed by an electrolytic cell, as stated by (Koponen, 2015). The reversible cell voltage (E_{rev}) denotes the

lowest voltage required for water electrolysis. This voltage can be determined under standard conditions (25°C and 1 bar) as outlined below:

$$E_{\text{rev}} = \frac{\Delta G}{zF} \quad (3.7)$$

$$E_{\text{rev}} = \frac{237.22 \frac{\text{kJ}}{\text{mol}}}{2 * 96485.3365 \frac{\text{C}}{\text{mol}}} = 1.23 \text{ V}$$

In the case where heat generation, thermal energy, or absorption are absent, the minimum voltage needed for water decomposition in a perfectly insulated electrolyzer is known as the thermoneutral voltage E_{tn} (Ebbesen et al., 2014). In an ideal electrolysis process, the thermoneutral voltage (E_{tn}) corresponds to the change in enthalpy. E_{tn} can be described as follows:

$$E_{\text{tn}} = \frac{\Delta H}{zF} \quad (3.8)$$

$$E_{\text{tn}} = \frac{285.840 \frac{\text{kJ}}{\text{mol}}}{2 * 96485.3365 \frac{\text{C}}{\text{mol}}} = 1.48 \text{ V}$$

The enthalpy change (ΔH) is minimally influenced by temperature, whereas $T\Delta S$ is significantly impacted by it. This results in the reversible voltage being more temperature-sensitive than the thermoneutral cell voltage. Because enthalpy is only slightly affected by temperature, higher operating temperatures reduce the amount of required electricity and allow for greater utilization of heat (Hu et al., 2022). Figure 6 illustrates the theoretical impact of temperature on cell voltage.

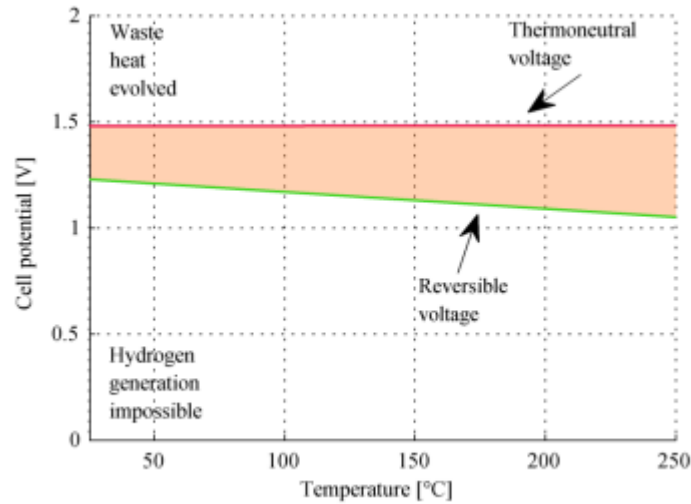


Figure 6 Relationship between temperature and cell voltage of Alkaline electrolysis (AEL) (Koponen, 2015)

According to figure 7, an increase in the electrolyte temperature reduces reversible voltage required to break down water molecules. As previously mentioned, the minimum Erev needed for water reaction is 1.22 V and if the cell voltage falls below this reversible voltage, the reaction does not occur (hydrogen generation is impossible). However, if the cell voltage is above the thermoneutral voltage (1.48 V), the electrolysis is exothermic, therefore excess heat is generated. According to Wei, Li et al (Li et al., 2022), all practical low temperature electrolyzers operate at voltage above thermoneutral voltage (1.48 V), thus producing waste heat. When the voltage lies between the reversible voltage and the thermoneutral voltage, electrolysis is endothermic, meaning the cell continuously consumes heat from its environment. If the reaction would happen in endothermic zone, the efficiency would be 100 % according to (Koponen, 2015) and the reaction would occur by absorbing heat from environment. Considering thermodynamic principles, it is beneficial to perform water electrolysis cell at elevated temperature. This occurs because a significant portion of the needed energy is supplied as thermal energy ($T\Delta S$), which significantly lowers the primary electrical energy demand (ΔG).

3.4 Electrochemistry of water splitting

The rate of hydrogen production correlates directly with the electric current flowing across the electrodes. Michael Faraday's two laws of electrolysis explain this relationship: Firstly, the extent of chemical transformation happening at the boundary between the electrolyte and the electrode correlates directly with the quantity of electricity applied. Furthermore, the quantity of chemical transformation caused by the identical quantity of electricity in different substances is directly related to their corresponding equivalent masses (Koponen, 2015). In the electrolysis mechanism, the cell voltage (E) constitutes the reversible voltage combined with any additional overvoltage present within the cell, and can be expressed as follows:

$$E_{\text{cell}} = E_{\text{rev}} + E_{\text{act,c}} + E_{\text{act,a}} + E_{\text{ohm}} + E_{\text{con}} + E_{\text{diff}} \quad (3.9)$$

Where E_{cell} represents the cell voltage, while $E_{\text{act,a}}$ and $E_{\text{act,c}}$ represent the anode and cathode activation overpotentials. E_{ohm} represent the overpotential attributed to ohmic losses within the cell components, while E_{con} is overvoltage caused by electrolyte concentration. The diffusion overvoltage E_{diff} becomes more significant at higher current densities, as it has minimal impact on alkaline electrolysis at relatively lower current densities (Jang et al., 2021).

E_{rev} , at any given temperature and pressure can be determined using the following equation:

$$E_{\text{rev}} = E_{\text{rev}}^{\circ} + \frac{RT(K)}{2F} \ln \left(\frac{(P - P_{v,KOH})(P - P_{v,KOH})^{0.5}}{a_{H_2O,KOH}} \right) \quad (3.10)$$

Where E_{rev}° is a standard equilibrium potential, P is pressure, T is the operating temperature, and R refers to gas constant. $P_{v,KOH}$ represent the pressure vapor of the solution, while $a_{H_2O,KOH}$ denotes the water activity of the potassium hydroxide salute. E_{rev}° is greatly affected by temperature and is expressed as following (Sakas et al., 2021):

$$E_{\text{rev}}^{\circ} = 1.5184 - 1.5421 \cdot 10^{-3} T(K) + 9.526 \cdot 10^{-5} T(K) \ln(T(K)) + 9.84 \cdot 10^{-8} T(K)^2 \quad (3.11)$$

The vapor pressure of the solution $P_{v,KOH}$ and P_{v,H_2O} are estimated based on the following equations:

$$P_{v,KOH} = \exp(2.302 a + b \ln(P_{v,KOH})) \quad (3.12)$$

$$P_{v,H_2O} = 10^{5.1962 - \frac{1730.63}{233.426 + T}} \quad (3.13)$$

Where T is operational temperature and a and b are expressed as experimental coefficients, and are determined as follow:

$$a = -0.0151 M - 1.6788 \cdot 10^{-3} M^2 + 2.2588 \cdot 10^{-5} M^3 \quad (3.14)$$

$$b = 1 - 1.2062 \cdot 10^{-3} M + 5.6024 \cdot 10^{-4} M^2 - 7.8228 \cdot 10^{-6} M^3 \quad (3.15)$$

The water activity of the potassium hydroxide salute $a_{H_2O,KOH}$ is denoted as follows (Sakas et al., 2021):

$$a_{H_2O,KOH} = \exp\left(-0.05192 M + 0.003302 M^2 + \frac{3.177 M - 2.131 M^2}{T(K)}\right) \quad (3.16)$$

Activation overpotential (E_{act}) is associated with the activated energy and it is caused by the electrochemical reaction. As reactions occur at the cathode and anode, they encounter an energy barrier that must be overcome for the reaction to proceed. Overcoming this barrier necessitates additional energy to facilitate the reaction. Activation overpotential relies greatly on the electrochemical activity of the electrode material and it is believed that E_{act} logarithmically grows with the current density (Hu et al., 2022). Based on (Sakas et al., 2021) literature, activation energy can be calculated as follows:

$$E_{act} = s \log\left(\left(\beta_1 + \frac{\beta_2}{T} + \frac{\beta_3}{T^2}\right) i_{cell} + 1\right) \quad (3.17)$$

Where β_1 , β_2 , and β_3 are model parameters and they describe the effect of activation overvoltage by considering the impact of current density and temperature.

The overvoltage appearing in the cell are illustrated in Figure 7 excluding the concentration overvoltage due to being much lower relatively to other overvoltage.

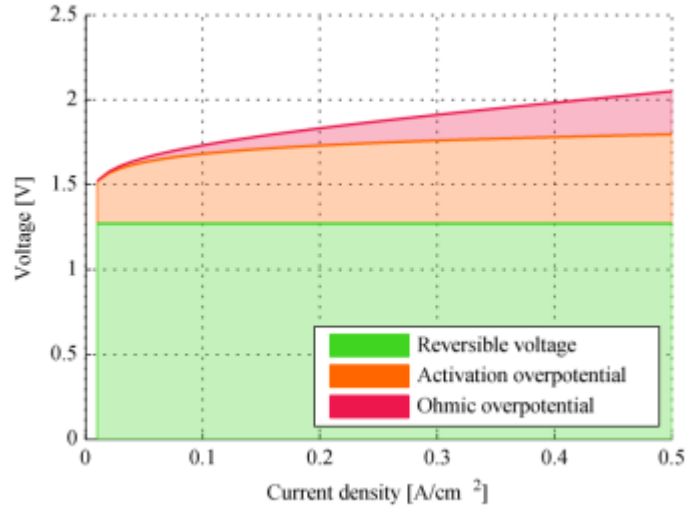


Figure 7 Overvoltages as a function of current density in AEL at temperature of 75 °C and pressure of 30 bar (Koponen, 2015).

According to ohms law, the electrical resistances serve as primary contributors to heat generation within the alkaline electrolysis cell, leading to the wastage of electrical energy in the form of heat formation (Zeng & Zhang, 2010). These electrical resistances encompass various factors, including resistance within the system circuit, opposition to the flow of ions in the electrolyte, formation of gas bubble on the electrode surfaces, and the presence of a diaphragm. The total resistance in AEL can be illustrated as follows (Santos et al., 2013):

$$R_{\text{total}} = R_{\text{electric}} + R_{\text{anode}} + R_{\text{bubble,O2}} + R_{\text{ions}} + R_{\text{membrane}} + R_{\text{bubble,H2}} + R_{\text{cathode}} \quad (3.18)$$

Ohmic losses refer to the energy lost due to electrical and transport resistances in the cell. This encompasses diaphragm resistance, bubbles resistance, and ionic transfer resistance. A comprehensive understanding of these resistances is crucial for enhancing efficiency in alkaline electrolysis (Santos et al., 2013). The magnitude of ohmic loss is mainly associated with electrical current passing through the cell. Ohmic overpotential can be determined by following equations (Sakas et al., 2021).

$$E_{ohm} = IR_{cell} \quad (3.19)$$

$$E_{ohm} = (\alpha_1 + \alpha_2 T) i_{cell} \quad (3.20)$$

Where, I represent the current flow, R_{cell} stands for the ohmic resistance of the cell, α_1 and α_2 are model parameter that explain the linear increase of ohmic overvoltage with different current density and temperature. Ionic losses attributed to the electrolyte primarily contribute to the dominant ohmic losses. Specifically, in AEL, the area-specific ionic resistance can be expressed using the subsequent equation (Koponen, 2015):

$$R_{ions} = \frac{\delta_{el}}{\sigma_{el}(T,M)} \quad (3.21)$$

where σ_{el} is the ionic conductivity of the alkaline solution as a function of temperature T and molarity M and δ_{el} is the thickness of the electrolyte layer.

The formation of gas bubbles within an electrolysis cell can result in significant overpotential if these gas bubbles are not removed rapidly enough. The coverage of these bubbles hinders effective contact between the electrode and the electrolyte, thereby stopping electron transfer and leading to an increase in overall ohmic loss for the whole system. On the electrode surface, bubbles gradually enlarge until reaching a critical size, causing detachment from the electrode surface (Santos et al., 2013). The existence of bubbles on the electrode surface and within electrolyte causes additional resistances to both the electrochemical reaction and ionic transfer, increasing electrical resistance because of lower conductivity of the gas. This contributes to the overall energy loss of the system. The reduction in electrical conductivity can be expressed as follows, as proposed by Bruggeman (Koponen, 2015):

$$\frac{\sigma_{\varepsilon}}{\sigma_o} = (1 - \varepsilon)^{1.5} \quad (3.22)$$

where σ_{ε} represents the conductivity in presence of gas bubbles, σ_o signifies the conductivity in the bubble-free electrolyte, and ε denotes the void fraction in the electrolyte. Various strategies have been proposed to tackle challenges associated with gas bubbles. One method involves decreasing the electrolyte's surface tension by employing surfactants, which helps in separating bubbles from the electrodes. Another strategy involves mechanically circulating the electrolyte, which speeds up the removal of gas bubbles. Additionally, applying appropriate coatings to the electrode surface to mitigate its hydrolytic properties serves as another effective solution (Santos et al., 2013). As mentioned earlier, zero-gap geometries can also mitigate bubble formation, thereby diminishing ohmic losses and potentially improving cell efficiency (Koponen, 2015).

3.5 Gas solubility

The available experimental data and literature regarding the solubility of oxygen and hydrogen under electrolysis conditions in concentrated KOH solution are quite limited. However, understanding the estimation of gas-liquid transfer in alkaline electrolysis necessitates knowledge of the solubility of gases in the electrolyte solution. It is well established that the product gas solubilities are higher in a lower concentrated electrolyte compared to higher concentrated electrolyte (Brauns & Turek, 2020). When there's an instantaneous change in hydrogen production rate, it leads to an instability in the partial pressure of the product gas, potentially resulting in supersaturation (Jang et al., 2023). Figure 8 illustrates the relationship between product gas solubilities and temperature in a 30wt% potassium hydroxide solution. The graph indicates that oxygen solubility decreases with temperature, whereas hydrogen solubility increases with temperature.

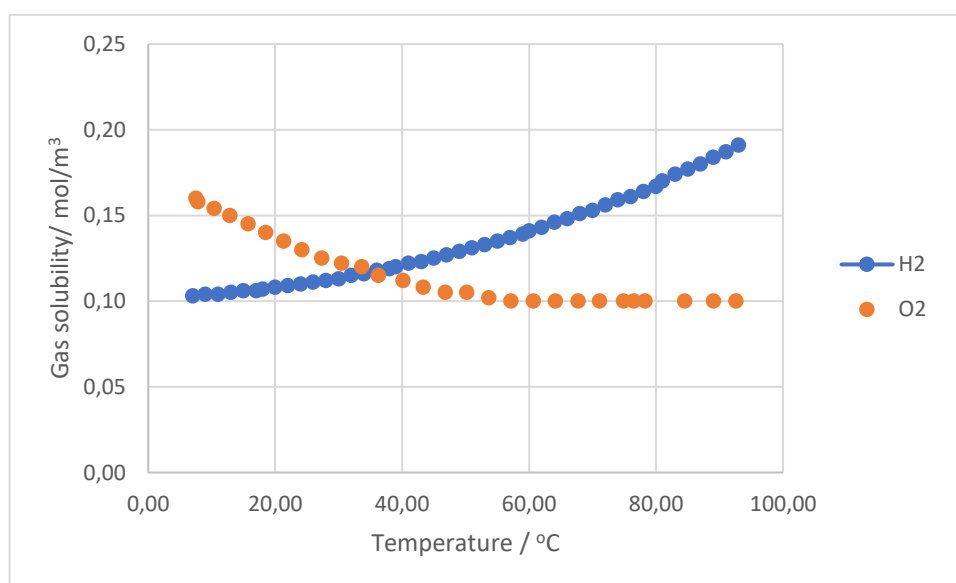


Figure 8 Hydrogen and oxygen solubility comparison at pressure of 1 bar and concentration of 30wt% KOH (Haug et al., 2017).

In comparison to oxygen, hydrogen exhibits greater solubility in the electrolyte. This is consistent with the principle of electrolysis reaction, which indicates that hydrogen is produced at a rate twice as fast as oxygen (Hu et al., 2022). As reported by Jang et al., the solubility of hydrogen in potassium hydroxide aqueous solution is roughly 3 times higher than that of oxygen (Jang et al., 2023). The graph below depicts the solubilities of product

gases across varying potassium hydroxide concentrations. It's evident from the figure that as the KOH concentration increases, the solubilities of product gases decrease notably.

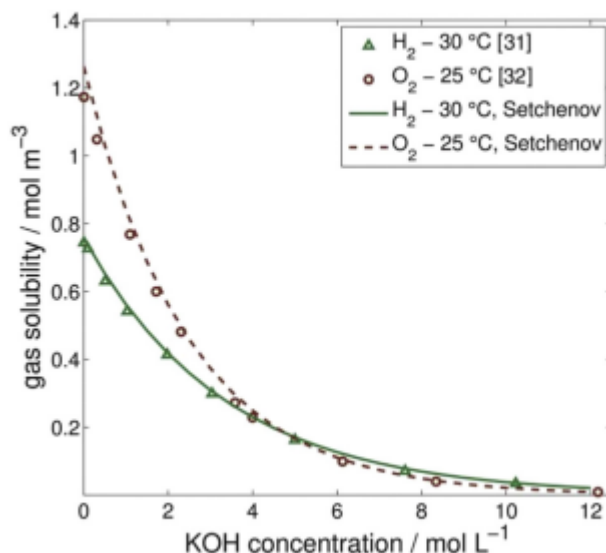


Figure 9 Modelled hydrogen and oxygen solubility compared to measured gas solubilities at 1 bar and temperature between 25 °C and 30 °C (Haug et al., 2017).

As temperature increases, the diffusion coefficients of product gases within the electrolyte solution decreases. Consequently, higher temperatures lead to a decrease in gas solubility, resulting in a reduction of gas impurities. Conversely, elevated pressure levels increase gas solubility, thereby increasing the diffusion of impurity gases (Hu et al., 2022).

Table 3. Solubility of hydrogen and oxygen (Hu et al., 2022)

Gas	Temperature (°C)	Electrolyte concentration	Solubility (mol/m ³)
H ₂	30	0.0091-10.23 mol/L KOH	0.7446-0.0344
H ₂	75	30.2 wt% KOH	0.088
H ₂	80	H ₂ O	0.753
O ₂	80	11.1 mol/L NaOH	0.0093
O ₂	25	H ₂ O	1.26

3.6 Alkaline electrolysis efficiency

There are several methods for stating the efficiency of electrolysis, each depending on the criteria used for evaluation and comparison. The voltage efficiency of an AEL can be represented by the following equation:

$$\eta_{\text{VOLTAGE}} = \frac{E_{\text{anode}} - E_{\text{cathode}}}{E_{\text{cell}}} \quad (3.23)$$

where E_{cathode} and E_{anode} are the potential at the cathode and anode. Conversely, thermal efficiency and Faradic efficiency are determined by evaluating the energy alteration in water electrolysis reaction. The energy input considered in these efficiencies are enthalpy change and Gibbs free energy change, which can be computed as follows (Santos et al., 2013):

$$\eta_{\text{thermal}} = \frac{\Delta H}{\Delta G + \text{Losses}} = \frac{E_{\Delta H}}{E_{\text{cell}}} \quad (3.24)$$

$$\eta_{\text{faradic}} = \frac{\Delta G}{\Delta G + \text{Losses}} = \frac{E_{\Delta G}}{E_{\text{cell}}} \quad (3.25)$$

Faraday efficiency is a ratio between the actual and theoretical maximum amount of hydrogen generated in the electrolyzer (Koponen, 2015). It examines the electrolysis process, while thermal efficiency considers the entire thermal equilibrium. Similar to the polarization curve, Faraday's efficiency can be represented by an empirical equation for a given specific temperature.

$$\eta_{\text{faradic}} = \frac{i^2}{f_{11} + f_{12} T + i^2} (f_{21} + f_{22} T) \quad (3.26)$$

Where T is operating temperature, and $f_{11}, f_{12}, f_{21}, f_{22}$ are coefficients. The hydrogen production rate can be calculated using Faraday efficiency as follows:

$$f_{\text{H}_2} = \eta_F \frac{N_{\text{cell}} I_{\text{cell}}}{zF} \quad (3.27)$$

where I_{cell} is the cell current and N_{cell} is the number of cells. The volume one mole of ideal gas occupied is corresponded to 22.41 number found in equation (3.21) at standard pressure and temperature. Specific energy consumption can be determined using the number of cells in the electrolysis N_{cell} , the cell current I_{cell} , and Cell voltage E_{cell} . The equation is expressed below (Koponen, 2015):

$$E_s = \frac{\int_0^{\Delta t} N_{cell} I_{cell} E_{cell} dt}{\int_0^{\Delta t} f_{H_2} dt} \quad (3.28)$$

The efficiency of an electrolyzer is established by comparing the energy content of the generated hydrogen to the electrical energy consumed for electrolysis, as well as for operating all necessary auxiliary equipment (pump, gas separators etc.). Using the specific energy consumption E_s , which considers only the electrolysis process, the electrolyzer efficiency can be expressed as following:

$$\eta_E = \frac{HHV_{H_2}}{E_s}, \quad (3.29)$$

where HHV_{H_2} is hydrogen higher heating value, which is equal to 39.4 kWh/kg. The efficiency of electrolyzer can also be determined as follows (Koponen, 2015):

$$\eta_E = \frac{E_{HHV}}{E_{cell}} \quad (3.30)$$

4 High-pressure and high-temperature alkaline electrolysis

Conventional industrial alkaline electrolysis cells typically operate at temperatures below 100 °C. However, researchers and scientists (Lohmann-Richters et al., 2021) have discovered that raising the operational temperature of alkaline electrolysis can yield notable benefits. By elevating the process temperature, the electrolyte's ionic conductivity is augmented, leading to enhanced electrochemical reaction rates at the surface of the electrodes. Elevating the temperature also makes the system thermodynamically favorable and enhance the electrode reaction kinetics of alkaline water decomposition. The thermal balance is significantly affected by increased temperatures and high pressures, and it must exceed the thermal-balance voltage if there is no external heat source available. The thermal balance voltage is the lowest voltage needed to maintain the necessary temperature for electrolysis in the absence of external heating. However, at elevated pressure water vapor pressure increases which reduces the amount of liquid water present in the process. According to Hauch et al. (2008) this reduction poses a challenge since it may result to fast evaporation of water from the electrolyte solution. To counteract this issue, high pressure must be applied to compel water into the solution and keep the electrolyte in the liquid phase, thereby preventing excessive water evaporation.

As the cell pressure is increased, the gas bubble size diminishes, causing larger number of gases to dissolve into the electrolyte. Conversely, large gas bubbles have an adverse impact on the reaction, as they augment the system's resistance. The elevated operating pressure leads to a reduced system voltage, translating to a lesser energy requirement for the electrolyzer to generate hydrogen. However, the pressure increase diminishes the gas bubble size, facilitating easier passage of oxygen and hydrogen gases through the porous membrane and their intermixing (Agata, 2015). According to Yde, et al. (2013), the utilization of high pressure in alkaline electrolysis eliminates the necessity for hydrogen compression post-production, thereby entirely removing the compressor from the overall system. High-pressure electrolysis also leads to reduced size of tubing and components compared to traditional alkaline electrolysis setups (Yde et al., 2013). This size reduction creates an opportunity to modularize the electrolyzer concept. While high pressure and temperature have demonstrated significant benefits for alkaline electrolysis, they also present certain drawbacks. One such challenge is the difficulty in sourcing materials capable of

withstanding the elevated temperature involved. Additionally, at elevated pressures, maintaining control over the pressure of oxygen and hydrogen becomes challenging, increasing the risk of gas mixing, which can compromise safety and efficiency (Yde et al., 2013).

Operating alkaline electrolysis at elevated pressure and temperature offers additional advantages beyond enhanced ionic conductivity and reaction rates. These benefits encompass improved electrical efficiency, higher current density, and the production of pressurized hydrogen and oxygen. Collectively, these advantages lead, according to Yde et al. (2013) to a reduction in investment costs, thereby addressing one of the setbacks traditionally associated with alkaline electrolysis. For instance, in Europe, the cost of industrial electricity is approximately 50 to 100 €/MWh, while the cost of heat is around 10 to 15 €/MWh. Therefore, OPEX are less in elevated temperature AEL than for low-temperature electrolysis since high temperature AEL uses more heat and less electricity (Millet, 2015). Although elevated temperature and pressure have many advantages, Ganley (2009) found that the primary drawback of raising cell temperature was the reduced longevity of cell components such as electrodes and diaphragm which encountered the highly corrosive electrolyte.

4.1 Structure of alkaline electrolysis cell at elevated temperature and pressure

The effect of high pressure and temperature on alkaline electrolysis has been studied earlier by several authors including Yde et al. (2013), Ganley (2009), and Chatzichristodoulou et al. (2016). In his thorough experimental work on high pressure and high temperature AEL, Ganley (2009) investigated various aspects of the process. He utilized a cell container composed of nickel 400 (Monel alloy), consisting of 66.5% nickel, 31.5% copper, 1.2% iron, and 1.1% manganese. This material was selected for its corrosion resistance against elevated-temperature alkali hydroxide solutions. The electrolyte used in the experiment was a 19 M KOH solution.

In this experiment, a range of electrical currents from 45 mA to 1000 mA was employed. The cell was used within a temperature range of 35°C to 400°C and under total pressures varying between 0.1 MPa and 8.7 MPa. Throughout the study, Monel wire was consistently used as cathode material. Numerous anode materials were analyzed, including nickel, cobalt-

plated nickel, lithiated nickel, and Monel alloy to assess their impact on the cell under the harsh oxidizing conditions experienced on the anode surface. To isolate the electrode wires, Teflon sleeves were utilized, and flowing water was employed to prevent any failure or melting of the Teflon sleeves.

In the study by Ganley (2009), the electrolysis was examined within a temperature range of 200 °C to 400 °C and a pressure of 1 bar. It was expected, based on previous research, that as temperature increased, both ionic conductivity and surface reaction rates would also increase. As the temperature climbed, there was a decrease in the electrolytic terminal potential, and the solution became dehydrated due to the elevated temperature. At heightened pressures, water maintained its activity in the electrolyte, leading to a diminished terminal potential. The experiments were conducted at temperatures of 35, 80, 200, 250, 300, 350, and 400 °C. The outcomes revealed a significant decrease in electricity requirement as the temperature rose under elevated pressure. The most favorable results were achieved at a pressure of 8.7 MP And a temperature of 400 °C, using a Monel wire cathode and a cobalt-plated nickel anode, as highlighted in Ganley's study.

Chatzichristodoulou et al. (2016) published an article detailing their development of an AEL process capable of operating at 20 bar and 200 °C. Due to the high temperature requirements, the authors focused on creating corrosion-resistant high-temperature diaphragms. Their experiment utilized mesoporous ceramic membranes as the alkaline electrolysis diaphragm. These membranes facilitated ion movement through the diaphragm and immobilized potassium hydroxide through capillary forces. Additionally, gas diffusion electrodes were selected as the optimal electrode option to overcome transport limitations at large production rates with mesoporous ceramic membranes.

For the anode, a NiFeCrAl alloy foam was impregnated with polytetrafluoroethylene (PTFE) and Ag nanowires to reduce the oxidation rate during the oxygen evolution reaction (OER). Conversely, Nickel foam coated with Inconel was utilized as the suitable hydrogen electrode at the cathode. The evaluation of this setup required 400 hours of continuous electrolysis at 20 bar and 200 °C. The results of the experiment indicated a significant reduction in investment costs by employing foam-based alkaline electrolysis cells (FobAECs) at 20 bar and 200 °C as an alternative of conventional alkaline electrolysis. Furthermore, the study demonstrated an improvement in production rates, leading to reduced hydrogen production compared to conventional AEC systems (Chatzichristodoulou et al., 2016)

4.2 Construction materials and corrosion stability

Conventional alkaline electrolyzers, typically operating at temperatures below 80°C, often utilize steel and nickel-plated steel as structural materials. However, at temperatures exceeding 90 °C, the alkaline electrolyte may initiate either normal or stress corrosion in metal materials. The conditions within an alkaline electrolyzer are highly corrosive, also due to the concentration of potassium hydroxide in the electrolyte. This corrosive environment is further compounded by the existence of O₂ at the anode and H₂ at the cathode, which initiates reactions on both sides. These reactions can cause materials such as electrodes to react with the electrolytes, leading to corrosion and degradation. Corrosion poses a significant challenge for electrolyzer components in terms of both metal contamination, which can poison the electrodes, and structural risk (Allebrod et al., 2012). According to Ursua et al. (2012), Corrosion tests reveal that austenitic stainless steel can withstand the potent oxidizing properties and high flammability of hydrogen up to temperatures of 120°C. Nickel and its alloys, while relatively expensive, can endure even higher temperatures. Nickel demonstrates resistance to both normal and stress corrosion and it's known for its relatively high activity and chemical stability. Nevertheless, the mechanical design of equipment must be meticulously considered, as nickel can cause gap corrosion at elevated temperatures.

Research on the material's performance at elevated temperature AEL, compared to conventional systems, remains limited. According to Lohmann-Richters et al. (2021), one of the principal challenges in high temperature and pressure AEL is the identification of suitable materials capable of withstanding not only high pressure and temperature but also extremely caustic environments. This emphasizes the critical need for continued research and development in materials science to advance high-pressure and high-temperature electrolysis technologies.

In numerous experiments, pure nickel has been utilized as an electrode material, thanks to its high active surface area and porosity. Most electrode materials, including metal oxides and alloys, have been examined at temperatures of up to 260 °C and according to Ebbesen et al. (2014), conventional nickel electrode appeared to withstand the temperature. In Ganley's (2009) experiment, various anode electrode materials, such as nickel, Monel wire, lithiated nickel, and cobalt-plated nickel wires, were evaluated at a temperature of 400

degrees Celsius and 8.7 MPa. The most favorable cell performance was observed using cobalt-plated nickel as the anode for OER and Monel wire as the cathode for HER under the above-mentioned conditions. PTFE and PFA were also tested and found to be suitable for high temperatures, although not for high pressure. Alloy 600 or Inconel alloy 600 was identified as the most promising vessel material, exhibiting superior resistance compared to other metals. (Yde et al., 2013)

Diaphragms are porous inorganic separators that are permeable to potassium hydroxide solution. They are primarily employed to stop the spontaneous recombination of reaction products, which primarily consist of hydrogen and oxygen, and they serve as ionic conducting materials. Today, Zifron has become a widely utilized membrane material. It comprises a porous composite structure composed of a polysulfone network combined with powdered zirconium dioxide (ZrO_2). In low temperature electrolyzers, nickel oxide, polymers, and asbestos are also effective, but both asbestos and polymers become unstable at temperatures exceeding 120 degrees Celsius. At elevated pressure, where oxygen becomes extremely soluble in the electrolyte, separating the product gases becomes increasingly crucial. The construction materials for electrolyzers operating at high temperatures and pressures must endure the enhanced corrosion associated with elevated temperature operations. Oxide ceramic separators, such as ceramics of titanates ($CaTiO_3$ and $BaTiO_3$), and even NiO, may serve as suitable alternatives for polymers and asbestos, but their stable operation at temperatures exceeding 200 degrees Celsius has yet to be conclusively proven (Hauch et al., 2008). Diaphragms crafted from composite materials, notably ceramics or microporous materials, have proven to be effective at elevated temperatures. In an experiment by Chatzichristodoulou, Allebrod et al. (2016), it was found that mesoporous ceramic diaphragms, with a thickness of 200 μm , were a suitable choice for operating at temperature of 200 °C and pressure of 20 bar.

In high-temperature AEL, most of the catalysts do not perform well due to inadequate stability under harsh elevated temperature conditions. Cobalt oxides have been shown to remain stable for OER up to 160 degrees Celsius, while for HER, molybdenum and titanium-stabilized Raney nickel have proven stable at the same temperature. Investigations have been conducted to assess the stability of different polymers under high-temperature and high-pressure alkaline electrolysis conditions. PTFE, PEEK, and PEEK + CA have undergone testing as cell frames in a 25 % KOH solution at 120 °C, demonstrating no signs of

degradation. According to (Lohmann-Richters et al., 2021), both PFA and PTFE exhibited no signs of degradation in concentrated potassium hydroxide at temperatures between 120 °C and 230 °C. Despite being suitable for elevated temperatures, PTFE and PFA can achieve even greater stability at higher temperatures when used in combination with fillers, such as glass fibers.

Based on the limited available literature, pure nickel, and alloy 800 have emerged as the most promising materials at 200 °C. However, Lohmann-Richters et al. (2021) stated that alumina and stainless steel have also shown potential at elevated temperatures. Nevertheless, these two metals require a low concentration electrolyte, typically ranging from 0.01 to 1 M, and lower current density of 45 mA cm⁻². Alloy 800, comprised of 33% nickel, 21% chromium, and 40% iron, along with iron passivated nickel, exhibit promising stability up to 200 °C. Similarly, Alloy 400, comprising 67% nickel, 31.5% copper, and 1.2% iron, could be a suitable material for laboratory-scale applications. Although, in Ganley (2009) experiment, nickel and cobalt-plated nickel demonstrated exceptional corrosion resistance a pressure of 8.7 MPa and a temperature of 400 °C, additional research and experimentation are required to ascertain their long-term viability.

Table 4. Conventional alkaline electrolyzer (La Camera, 2020) and potential properties and materials for high pressure and temperature alkaline electrolyzer (Lohmann-Richters et al., 2021)

Temperature (°C)	70 – 90	150 – 200
Pressure (bar)	1 – 30	10 – 50
Current density A m ⁻²	< 6000	37500, <1.8 V
Electrolyte	KOH	KOH
Anode/catalyst	Perforated stainless steel coated with nickel	mixed oxide Ni, Fe or Co
Cathode/catalyst	Perforated stainless steel coated with nickel	Raney-Ni-Mo
Diaphragm	ZrO ₂ stabilized with PPS mesh	porous zirconia < 100 μm thick
Polymer parts	PSU, PTFE, or EPDM	PTFE

5 Cost of alkaline electrolysis

Alkaline electrolysis stands out as an appealing method for hydrogen production, boasting high efficiency and the capacity to operate under high pressure. More significantly, it is viewed as a key player in addressing global decarbonization challenges. Despite these advantages, the widespread adoption of hydrogen production through alkaline electrolysis remains limited in the global market, primarily due to the substantial costs associated with capital expenditure and electricity consumption (Xu et al., 2020). The investment cost estimations of AEL depend mostly on plant size (Kuckshinrichs et al., 2017) and the cost of AEL system can be separated into two main types: capital expenditure (CAPEX) and operational expenditure (OPEX). As for every industrial company, CAPEX holds significant importance in determining the overall economic feasibility of the industry. For alkaline electrolysis, CAPEX is extremely important to its competitiveness and success against other water electrolysis methods. CAPEX is heavily influenced by different equipment used, while electrical efficiency determines the OPEX associated with carrying out the electrochemical reaction. CAPEX encompasses the expenses associated with purchasing and installing the entire alkaline electrolysis system, along with construction costs. Conversely, OPEX covers utility expenses, such as electricity, water supply, labor, and the costs of stack replacement (Song et al., 2023).

Estimating the cost of Alkaline Electrolysis (AEL) proves challenging due to variations in technology, materials, and production scale. The dynamic nature of AEL production further complicates cost calculations, with the costs of electrolyzers changing rapidly (Marian et al., 2022). Notably, the costs of AEL have witnessed a significant decline in recent years, attributed to strategic cost reduction measures implemented by both governments and companies. This reduction in costs is instrumental in lowering overall investment expenses (La Camera, 2020). It is believed that as the AEL production level increases, the costs of stack increase too, however this increase is more associated in smaller capacity installations. The real cost reductions are seen in the balance of plant. To achieve stack cost reduction, using less critical and expensive materials and increasing current densities are viable strategies (Marian et al., 2022).

5.1 Cost structure of alkaline electrolysis

In general, an alkaline electrolysis system is composed of the electrolyzer stack and the balance of plant. The stack serves as the site for the electrochemical process of hydrogen production, housing essential components such as two electrodes (cathode and anode), a diaphragm, seals, frames, and end plates to avoid leaks and manage fluids effectively. Conversely, the balance of plant extends beyond the stack and encompasses various components such as power conditioning (involving transformers and rectifiers for supplying DC electricity), a control system, hydrogen conditioning (including gas separation, pressurization, and drying), water supply (involving purification and heating), and electrolyte circulation. Unlike other electrolysis methods, alkaline electrolysis necessitates pressure management to maintain equilibrium between O₂ at the anode and H₂ at the cathode (Genevieve, 2008).

In 2017, the reported capital cost for alkaline electrolysis system ranged from 800 €/kW to 1300 €/kW including only CAPEX (Schmidt et al., 2017). However, various literature sources on alkaline electrolyzers present different capital cost variations. Academic estimation and multiple references sources were used to evaluate the CAPEX and OPEX of alkaline electrolysis. As of 2022, Marian et al. (2022) indicate that the CAPEX for alkaline electrolyzers ranges from 170 €/kW to 1000 €/kW. Notably, the minimum cost of 170 €/kW is noteworthy, attributed to findings from various Chinese industrial plants. Typically, OPEX constitutes 2 to 4% of the initial CAPEX excluding electricity costs. According to estimations by (Marian et al., 2022), the OPEX for Alkaline Electrolysis (AEL) falls between 3.4 €/kW and 20 €/kW to 6.8 €/kW and 40 €/kW, respectively. Since 2014, the capital expenditure (CAPEX) for large-scale electrolyzers has seen a significant decrease, dropping by over 45% from 2000 €/kW to 1200 €/kW, as reported by Marian et al. (2022).

Figure 10 depicts the evolution of the Capital Expenditure (CAPEX) cost of Alkaline Electrolysis (AEL) over the years, revealing a notable and rapid decline in costs in recent times. This significant cost reduction is attributed to the substantial increase in the production scale of alkaline electrolysis systems. The AEL system has witnessed a considerable expansion in plant size, growing from approximately 120 kW to 2 MW between 2010 and 2017. The impact of this change in scale is evident in the graph, illustrating a noteworthy decrease in CAPEX costs from 1700 €/kW in 2010 to 500 €/kW in 2017. Each

data point on the graph corresponds to an actual commercially available process, highlighting the tangible shifts in the economic landscape of AEL (Marian et al., 2022).

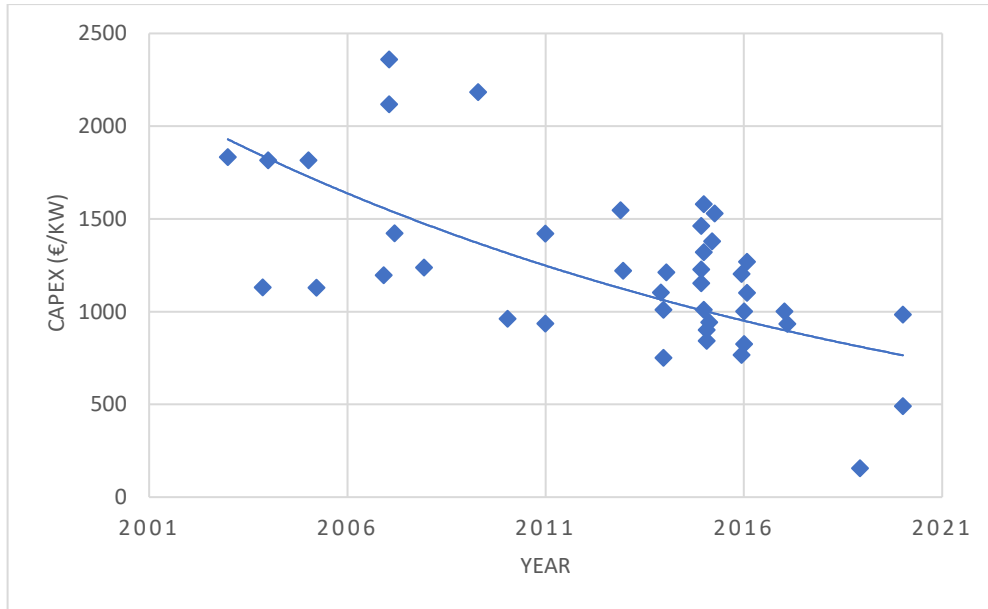


Figure 10 Alkaline process CAPEX costs over the years. Data collected from Marian et al. (2022)

Table 5 An illustration of a current conventional alkaline electrolysis process key parameters (Deloitte, 2021)

Key parameters	AEL plant
Overall	
Plant Scale (kg/day)	Up to 70 000
Purity (%)	99.7 – 99.9
Flexibility	
Start response (min)	Up to 10
Ramp-up / down (%/sec)	0.2 to 20
Shutdown Response (min)	Up to 10
Load Range (%)	10 -110
Operational Pressure (bar)	1 – 30
Operating Temperature (°C)	60 – 80
Lifetime	
Full system (year)	20
Stack (h)	75 000
Power efficiency	
Power consumption (kWh/kg H ₂)	48 – 53
Degradation (%/1000 h)	0.1
CAPEX	
Full system (€/kW)	750 – 1400
Stack (% of full system)	35
OPEX (without electricity)	
OPEX per year (%)	2 to 4

In 2020, the International Renewable Energy Agency (IRENA) conducted a comprehensive analysis of the cost breakdown for the alkaline electrolysis process (La Camera, 2020). According to their breakdown, the stack accounted for 45% of the overall system cost, while the balance of plant (BOP) constituted the remaining 55% of the overall process cost. The overall cost refers to the CAPEX of the system, where OPEX costs is accounted as 2 to 4 % of the total CAPEX. Figure 11 illustrates that within the BOP, the primary contributor to cost was the power supply, representing 50% of the total BOP cost. Following closely were

deionized water circulation at 22%, cooling (heat exchanger) at 8%, and hydrogen processing at 20%, which includes hydrogen purification, compression, and storage. Figure 11 further breaks down the stack cost, revealing that 57% of its total cost is attributed to the diaphragm and electrode package. Manufacturing plays a significant role in this cost component, claiming 71% of its total cost. This notable manufacturing share is a result of intensive efforts in producing and coating the electrodes with catalysts (Holst et al., 2021). It's essential to emphasize that the distribution of costs in the alkaline electrolysis breakdown can vary significantly across different literature sources. For instance, in the breakdown by Mayyas and Mann (2018), the balance of plant contributed 60% to the total system cost, while the stack constituted only 40% of the overall process cost.

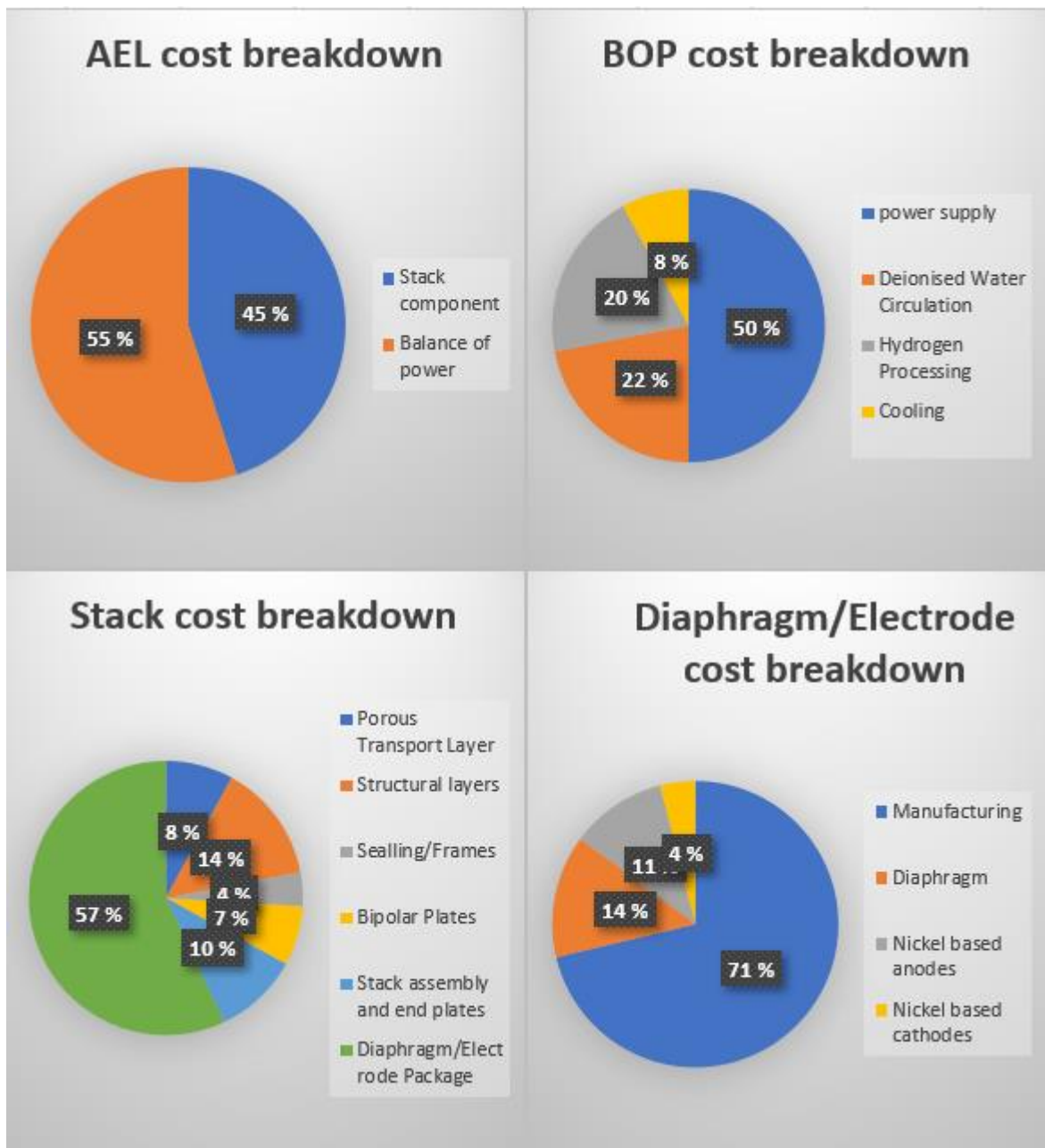


Figure 11 System, balance of plant, stack, and diaphragm/electrode cost breakdown for 1MW alkaline electrolyzer (La Camera, 2020)

Holst et al. (2021) developed a cost model specifically for a single 2.5 MW stack with the primary objective of estimating the investment cost of an alkaline electrolysis stack. The aim was to leverage stakeholder information and available literature to construct this cost model, focusing predominantly on the capital cost of fundamental components at the stack level. Notably, the breakdown did not include components associated with the balance of plant.

The specifics of this model include a cell area of 20,000 cm², comprising 116 cells per stack, operating at a current density of 6000 A /m². The operating conditions involved a pressure of 1 bar and temperature of 80°C, with a voltage and faradaic efficiency of 99% and 82%, respectively. Other pertinent cost properties considered in the model were the cell voltage (1.8 V), stack current and voltage (12,000 A, 208 V), hydrogen production stack (51.8 kg/h, 576 Nm³/h), and specific energy consumption (48.3 kWh/kg, 4.35 kWh/ Nm³).

Utilizing the parameter values provided above, Figure 12 delineates the cost model breakdown by Holst et al. (2021), revealing that half of the 2.5 MW stack cost is primarily attributed to electrodes (cathode and anode). Following closely, bipolar plates (BPP) constitute a substantial portion, accounting for 18% of the overall stack cost. Despite bipolar plates being typically crafted from cost-effective materials like stainless steel, the complexity in their geometry, as highlighted by Holst et al. (2021), renders them intricate and consequently expensive. Separators hold a 9% share, which might seem modest, but their crucial role in the stack's performance emphasizes their significance. The balance of stack (BoS) encompasses smaller components such as construction frame materials, fittings, and threaded rods, contributing to a 5% share of the total cost.

Upon comparing the 1 MW stack cost breakdown from IRENA (La Camera, 2020) and the 2.5 MW stack cost breakdown by Marius Holst and his team (Holst et al., 2021), a noticeable similarity emerges in the distribution of costs. Specifically, the share allocated to electrodes and diaphragm appears almost identical for both cost models. In the case of electrodes and separator, they jointly contribute to 71% (IRENA) and 68% (Marius Holst et al.) of the total stack cost.

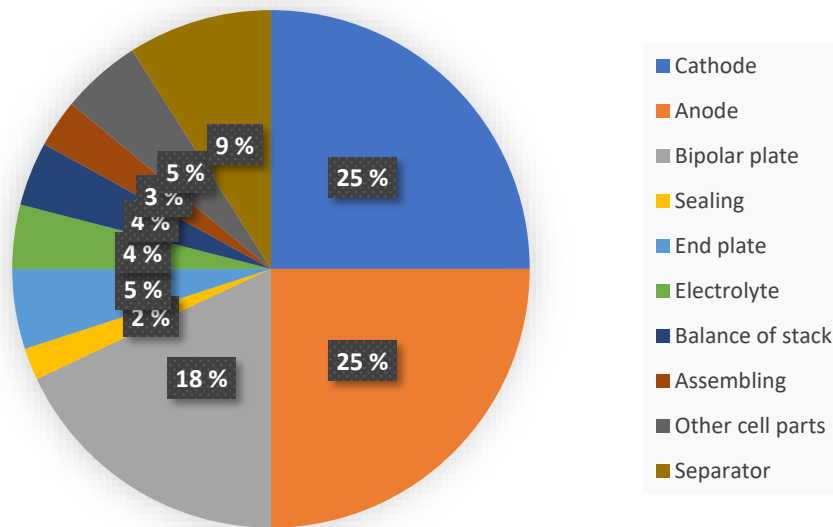


Figure 12. Cost breakdown illustration of 2.5 MW Alkaline electrolysis stack (Holst et al., 2021)

5.2 Economic analysis for conventional alkaline electrolysis

Jang, K et al. (2022) carried out an economic analysis of alkaline electrolysis, specifically for a 1MW hydrogen production plant. In this plant, a current density of 0.40 A/cm² and a cell voltage of 1.88 V were employed, resulting in a system efficiency of 65.75%, and a hydrogen production of 109.95 Nm³/h. The economic analysis was facilitated by making the following assumptions.

- The plant was assumed to operate only 12 hours a day, with a total lifetime of 20 years (approximately 80,000 hours) and a system degradation of 1.3 % over 10,000 hours. (Nguyen et al., 2019)
- No profit was expected in the first year, as it was considered the construction period.
- Because of small size of the plant, it was assumed that one full-time worker could effectively manage operations.
- The byproduct of the process was assumed to be sold for 0.054 \$/kgO₂ (Jang et al., 2022).
- A discount rate and income tax rate of 8 % and 30 %, respectively, were assumed.

- Start-up time, ramp up, ramp down, and minimum part load were estimated at 20 min, 7-17%/s, 10-25%/s, and 3-8% (Nguyen et al., 2019).

Figure 13 illustrates a graphic breakdown of cost for a 1MW alkaline electrolysis plant, including CAPEX cost, OPEX cost, and electricity. For the purposes of this analysis, the electricity cost was assumed to be 66.7 \$/MWh, based on the industrial electricity rates in Korea (Jang et al., 2022). According to (Nguyen et al., 2019) service and maintenance expenses make up 2 % of the total CAPEX, while other operating costs only account for 1 % of the total CAPEX cost. (Jang et al., 2022) also provides estimates for the price of electrolyte (KOH) and deionized water, which are 2.92 \$/kg and 0.01 \$/kg respectively. The cost for the electrolyzer stack contributes 40 % of the total CAPEX, while the BoP cost comprises the remaining 60 % of the CAPEX total cost. Table 6 categorizes the cost items associated with the hydrogen production plant and provides estimates for the items used in the AEL system. The total capital cost of the plant, which includes stack and balance of plant costs is estimated to be 0.74 M\$/MW (Jang et al., 2022).

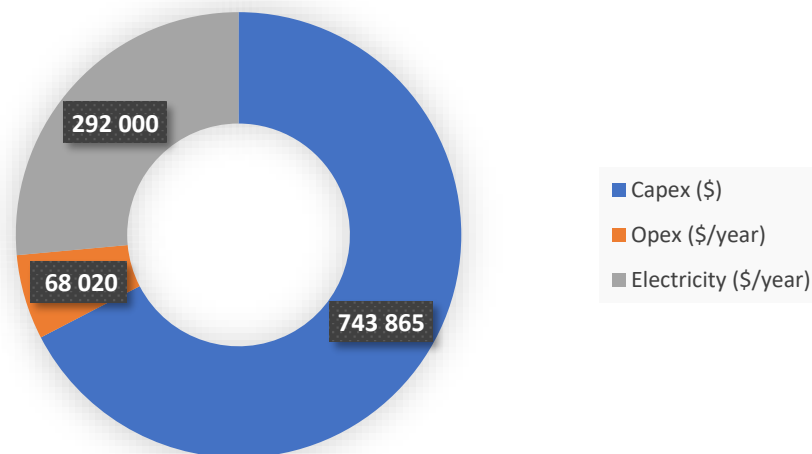


Figure 13 CAPEX, OPEX, and electricity cost share of 1 MW alkaline electrolysis

Table 6 Classification of cost components and production cost of hydrogen for 1 MW alkaline electrolysis plant (Jang et al., 2022)

	Items	AEL
Capital cost (\$)		
	Stack	340 000
	BOP	403 865
	Hydrogen processing	83 880
	Water circulation	87 082
	Power supply	198 225
	Cooling	28 678
	Other BOPs	6000
OPEX (\$/year)		
	Labor	36 575
	Water	8 649
	Electricity	292 000
	KOH	480
	Maintenance	14 877
	Other operating cost	7 439
Production rate of hydrogen (kg _{H2} /year)		86 488

5.3 High pressure and high temperature influence on cost of AEL

Elevated pressure and temperature play a significant role in enhancing electrolysis performance and, consequently, efficiency. However, the adoption of a high-pressure configuration introduces the need for more robust cell frames and balance of plant (BoP) materials, impacting the Capital Expenditure (CAPEX). Optimizing the utilization of active cell areas and enhancing current density can lead to a reduction in necessary materials and a decrease in capital expenditures (Koponen, 2015). The compressor's auxiliary equipment and the need of external gas (hydrogen and oxygen) compression can be eliminated by using the pressurized electrolyzer, which can therefore lead to the reduction of the investment and operational cost (Koponen, 2015). The advantages of high pressure extend to the reduction in gas volume and flow rate, subsequently minimizing equipment size. According to Allebort et al. (2012), the electricity needed to pressurize hydrogen using a compressor is approximately 5% higher than that required for pressurization by an electrolyzer. This implies that employing a high-pressure electrolyzer can lead to a reduction in electricity costs. In the realm of high-temperature Alkaline Electrolysis (AEL), an increase in temperature enhances current density, thereby elevating the hydrogen production rate, improving gas production efficiency, and mitigating energy waste through the utilization of generated heat for system heating. Consequently, this approach contributes to a reduction in investment costs and the overall size of the electrolyzer (Hu, Guo et al. 2022). It has been demonstrated that high-temperature AEL improves the electrical efficiency of the electrolyzer by minimizing electrical losses, such as ohmic overpotential, ultimately lowering hydrogen production costs (Allebrod et al., 2012).

Although alkaline electrolysis has long been a recognized technology commercially accessible for decades, the high-pressure and high-temperature (HPHT) alkaline electrolysis is comparatively new, with limited empirical data available regarding its capital expenditure (CAPEX) value. This is because commercial HPHT alkaline electrolysis systems are not yet widely available. (Xu et al., 2020) demonstrated the performance of a high-temperature alkaline electrolysis cell using lithium hydroxide (LiOH) as an electrolyte and a SrZrO₃-based matrix. The authors performed an economic analysis for a 1 MW elevated temperature AEL system based on the demonstrated cell performance, assuming 90% heat recovery from the electrolysis system. The system achieved a cell voltage of 1.35 V and a current density

of 10000 A/m² at 550°C. The estimated cell lifetime was 20 years, with a low electrical cost of 0.039 \$/kWh and a design capacity of 1500 kg H₂/day. The hydrogen production cost was calculated to be 2.59 \$/kg H₂, with an efficiency of 39 kWh/kg H₂. The overall hydrogen price, including distribution costs, was estimated to be 5.05 \$/kg for high-temperature alkaline electrolysis. The electricity price was assumed to be between 4-5 cents/kWh. Repeating stack components are active components that are involved in the electrochemical reaction that occurs during the electrolysis process and they include for instance electrodes and electrolyte. Non-repeating components on the other hand are non-active components such as gasket, seals, and end plates. The figure below illustrates the contribution of stack replacement and the balance of the plant in an elevated temperature AEL system.

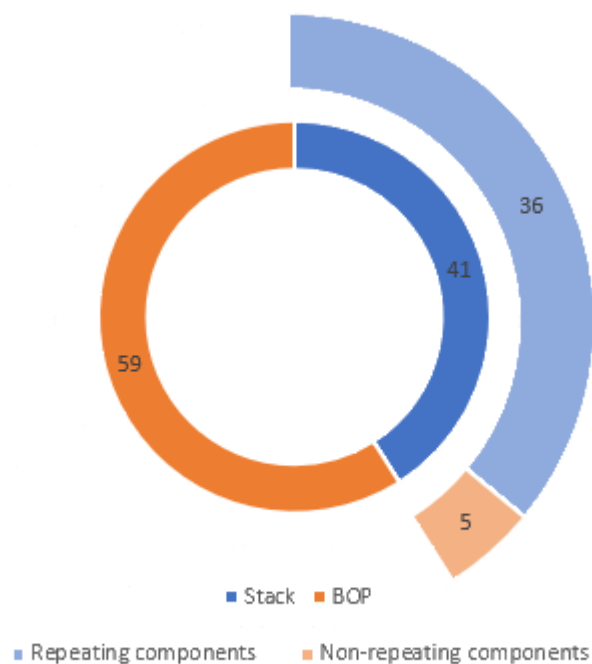


Figure 14 Capital cost breakdown for the 1 MW HT-AEL system (Xu et al., 2020).

Improving cell performance and adopting stable materials under harsh alkaline conditions, combined with utilizing affordable renewable electricity, is expected to reduce the cost of high-temperature alkaline electrolysis. Table 7 illustrates the contribution of hydrogen production costs in high-temperature alkaline electrolysis.

Table 7 Cost analysis for the 1 MW HT-AEL system (Xu et al., 2020)

H ₂ production cost contribution	HT alkaline cost (\$/kg)
Capital cost	0.38
Electricity	1.44 (39.3 kWh/kg H ₂)
Electrical cost (\$/kWh)	0.039
Fixed O&M	0.75
Variable costs	0.020
Hydrogen production cost (\$/kg)	2.59
Overall H ₂ price including distribution costs (\$/kg)	5.05
Design capacity (kg H ₂ /d)	1500

Table 8 presents a comparison of power consumption and energy efficiency between low-temperature, low-pressure alkaline electrolysis (80°C) and high-pressure, high-temperature alkaline electrolysis (200°C) at a current density of 5000 A/cm². The comparison aims to assess the impact of pressure and temperature variations on the electrolysis process. Analyzing both low and high-temperature conditions provides insights into potential advancements in the field. As indicated in Table 8, a notable decrease in power consumption and an increase in energy efficiency were observed when transitioning from 80°C to 200°C. This energy-saving tendency results from reductions in activation energy and internal resistance inside the electrolyzer. Consequently, there is also a decrease in reversible voltage, ohmic, and activation overpotential with rising temperatures.

Table 8 Power consumption and energy efficiency between LTP and HTP alkaline electrolysis (Nami et al., 2022).

	LTP-AEL	HTP-AEL
Total consumed power (kWh/kmol)	358	305
Energy consumption (MWh/t H ₂)	50	42
Energy consumption (kWh/Nm ³ H ₂)	4.5	3.8
LHV-based Energy efficiency (%)	66	79

6 Simulation

6.1 Objectives

This section aims to develop and simulate a 2.78 MW process model for alkaline electrolyzers. The objective is to comprehensively understand the impact of pressure and temperature on alkaline electrolysis. To delve deeper into this, an Aspen Plus model was employed operating at 16 bar and 80°C. Additionally, Excel calculations were conducted utilizing the equations provided in chapter 3.3. The following chapters detail process simulation, Excel calculation results, and economic analysis. For further reference, the equations utilized in this section can be found in Chapter 3.3.

6.2 Development of alkaline electrolysis process model

A comprehensive Aspen Plus model was created to assess the impact of temperature and pressure on alkaline electrolysis. This Aspen Plus model encompasses not only the alkaline electrolyzer reactor but also all other necessary auxiliary equipment, such as gas-liquid separators, compressors, dryer, DEOXO reactor, and more as delineated in Figure 16 of the process flowsheet. To perform the process modelling in Aspen Plus, the data needed were obtained from an industrial scale electrolyzer (Sakas et al., 2021). Table 9 provide the input for simulating the AEL plant under standard conditions. The model operates on a closed-loop circulation principle, whereby unreacted water and potassium hydroxide are recycled as input. In the model, a constant flow rate of 7.51 kg/s of deionized water is pumped every second through the pump, which increases its pressure to meet required pressure. The pressurized deionized water is fed to a liquid-gas separator (FLASH2), where oxygen is separated from the liquid solution comprising unreacted water and potassium hydroxide (KOH). Subsequently, any residual water and hydrogen present in the oxygen stream undergoes further purification in DEOXO reactor (DEOXO2), where hydrogen react with hydrogen to form water. Water is then removed in a dryer (Dryer2). Deionized water, along with remaining unreacted electrolyte, is directed to a mixer where it is blended with purified potassium hydroxide (KOH). Notably, KOH, being inert within the process, is introduced

sparingly and only when required. Subsequently, the solution is cooled in a heat exchanger before flowing the electrolyzer. After, the solution undergoes further mixing in another mixer, this time with electrolyte sourced from the hydrogen separation circle. The solution then flows to the isothermal reactor, serving as an electrolyzer. The isothermal reactor is used to simplify the Aspen plus simulation model by keeping the process at constant temperature.

The simulation utilized the RStoic reactor type, facilitating the split of H_2O into H_2 and O_2 . As water is consumed at the cathode, the water amount in the electrolyte decreases, leading to an increase in the electrolyte concentration. To prevent this, design specifications were implemented to maintain a constant amount of water and KOH in the system. Pump1 is designed to feed water into the system to replace the amount consumed during hydrogen and oxygen production, thereby maintaining the KOH concentration. Although KOH is not consumed in the process, small amounts need to be added periodically to maintain its concentration. Therefore, another design specification was made to add KOH to the system as needed.

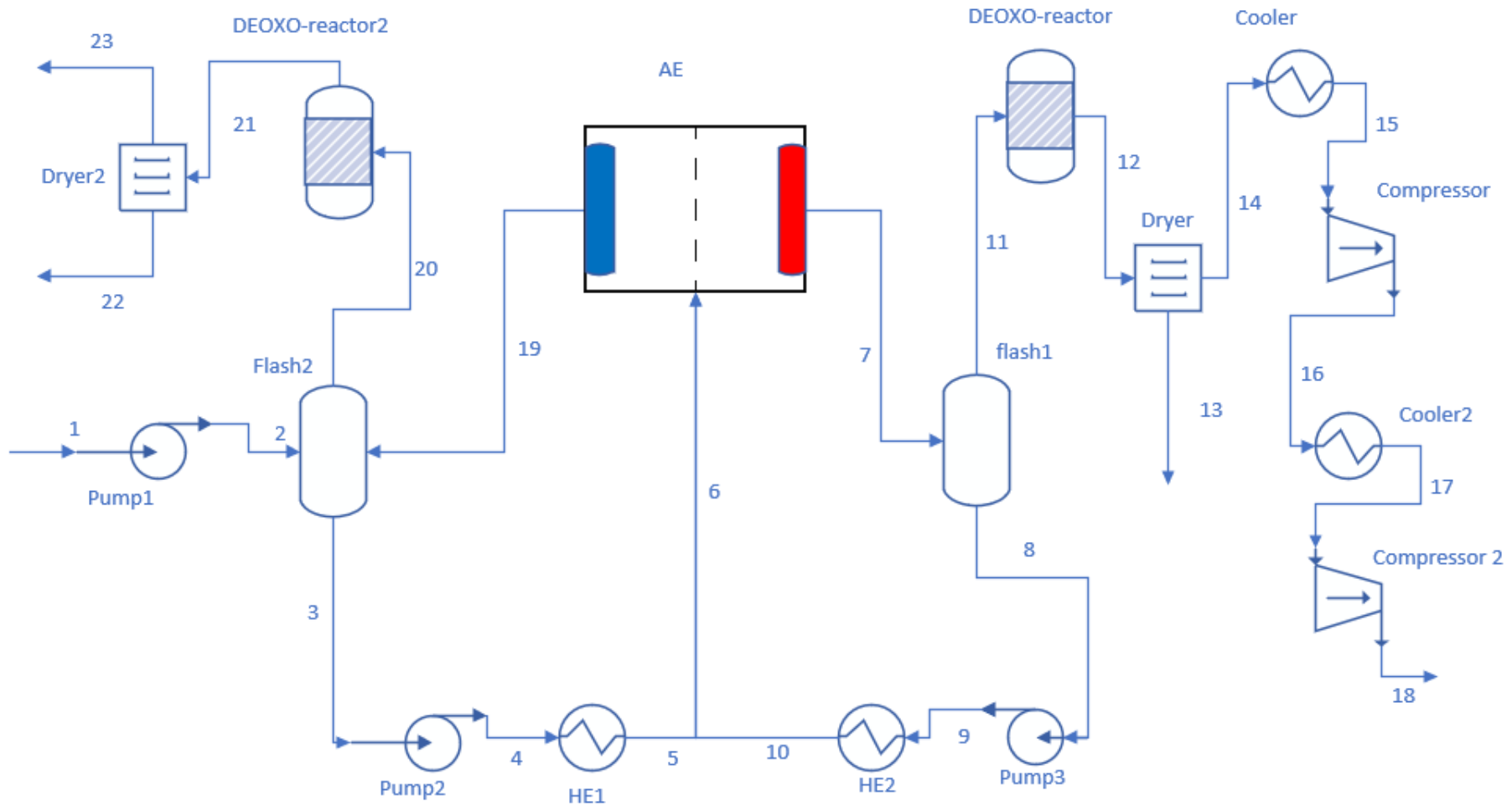


Figure 16 Process flow diagram of AEL

The produced gases and electrolyte then flow to the vapor-liquid separator (VAP-SEP), an additional conceptual unit. In Aspen Plus, this separator helps calculate the vapor volume fraction in the reactor's outlet stream. This volume fraction is used to adjust the water conversion in the water-splitting reaction to a level that matches practical conversion in the electrolysis cell. Although there is no detailed information on the vapor volume fraction in industrial processes, it can be assumed that a volume fraction of 50% should be close to reality. The vapor and liquid are then mixed again and sent to another conceptual separator (B4), where hydrogen and oxygen are separated for further treatment. It's important to note that in a commercial alkaline electrolysis, hydrogen and oxygen are separated in the electrolyzer, with oxygen generated at the cathode and hydrogen at the anode. During H₂ purification stage, hydrogen flows to a liquid-gas separator (FLASH1), where the electrolyte is removed and returned to the reactor. The purified hydrogen from the liquid-gas separator remains saturated with water and small amounts of oxygen, which need to be removed to ensure efficiency and achieve high-quality hydrogen. Therefore, the hydrogen is sent to a DEOXO reactor, which acts as an oxygen removal purifier. The DEOXO reactor eliminates oxygen from the hydrogen stream by facilitating an oxygen-hydrogen recombination reaction. The resulting water and hydrogen are then sent to a dryer to eliminate any residual moisture from the H₂ stream, ensuring that hydrogen gas is completely dry. Dried hydrogen is then compressed to 50 bar and stored for further use.

In the model, a reciprocating compressor was used instead of a centrifugal compressor for two reasons: first, the operational range of the reciprocating compressor is better suited for small flow rates; second, the centrifugal compressor has limitations with low hydrogen flow rates at low electrolyzer loading. Hydrogen compressors have temperature limits because high temperatures decrease compressor efficiency, requiring more energy to achieve the desired pressure. In the worst-case scenario, the compressor material can weaken, deform, or fail, leading to potential leaks or mechanical breakdown. The maximum discharge temperature for a reciprocating compressor is 150°C, and the temperature limit for hydrogen-rich gas is 130°C (Eduardo, 2011). To minimize the discharge hydrogen temperature, we used two reciprocating compressors with an intercooler between stages to lower the hydrogen temperature between stages.

The isothermal reactor (AE), which functions as the cell stack, serves as the central component of the system. A power input of 2.78 MW is applied to the reactor to initiate the electrochemical breakdown of H₂O into H₂ and O₂, as shown in equation (3.3). The cell stack consists of 326 cells, arranged horizontally with an area of 2.659 m². Table 9 shows the operation units used in Aspen Plus.

Table 9 System simulation input data under standard operating conditions (Sakas et al., 2021).

Parameter	Value
Temperature (°C)	80
Pressure (bar)	16
Cell area (m ²)	2.659
Cell number (cells)	326
Input power stack (MW)	2.78
Electrolyte circulation rate (kg/s)	10.44
Electrolyte (wt% KOH)	30

6.3 Energy and mass balance

From the data obtained from Aspen Plus, the system yields a pure H₂ production rate of 0.019 kg/s at a current density of 3500 A/m². This corresponds to a power requirement of 2.78 MW for the electrolyzer to decompose H₂O into H₂ and O₂ at 80°C and 16 bar. Additional utilities, such as compressors and pumps, consume 60 kW, bringing the total power requirement for the process to 2.84 MW.

Table 10 Mass flow composition under base-case operating conditions (80 °C, 16 bar)

Stream	T (°C)	p (bar)	Mass flow (kg/h)	Composition (kg/h)			
				H ₂ O	KOH	H ₂	O ₂
H ₂ OIN	25	1	27031.6	27031.6	0	0	0
H ₂ OFEED	26	16	27031.6	27031.6	0	0	0
RIN	80	16	71439	53405.1	18021.1	0.66	12.19
ROUT	80	16	71439	52781.2	18021.1	70.48	566.27
SEPH ₂	80	16	35477.4	26390.6	9010.5	70.14	6.09
SEPO ₂	80	16	35961.6	26390.6	9010.5	0.33	560.17
H ₂	80	16	92.63	17.11	1.5e-16	69.49	6.03
H ₂ -OUT	80	16	69.49	0	69.49	0	0
PURGE1	80	16	23.90	23.90	0	0	0
O ₂	80	16	556.93	8.566	7.7e-17	0.33	548.05
O ₂ -OUT	80	16	548.04	0	0	0	548.04
PURGE2	80	16	8.56	8.56	0	0	0
PURGE3	80	16	0.33	0	0	0.33	0

6.4 Equipment sizing

The equipment sizing has been done with Aspen Plus simulation. The inner diameter (d) of the pipes is determined using the following equation:

$$d = \sqrt{\frac{4Q}{V\pi}} \quad (7.3)$$

Where:

d represents the inner diameter of the pipe (m)

Q is volumetric flow rate (m³/s)

V is velocity of the fluid (m/s)

6.4.1 Separation unit

The separation unit (Liquid-gas separator) can be sized based on volumetric flow of liquid and residence time. The required height of the vessel to contain the specified liquid can be calculated using the following equation:

$$L_l = \frac{4Q_l}{\pi D_v^2} t_r \quad (7.4)$$

Where:

L_l is the height of the vessel.

Q_l is volumetric flow of liquid.

D_v is diameter of the vessel.

t_r is residence time.

Diameter of the vessel can be calculated from Eq. (7.3), where Q is volumetric flow of gas and V being gas velocity. The velocity of the gas can be determined as 2/3 times the amount of terminal settling velocity (V_t), which can be determined using Intermediate Law equation:

$$V_t = \frac{2.94g^{0.71}D_{\mu}^{1.14}(\rho_L - \rho_g)^{0.71}}{\rho_g^{0.29}\mu^{0.43}} \quad (7.5)$$

Where D_u is diameter of gas bubble, ρ_L is density of liquid, ρ_g is density of gas, and μ is viscosity of gas.

when volumetric flow and residence time is known, the vessel volume can be determined with the equation (7.6). The flowrate of the feed used in the calculation was 0.346 m³/s (Uki et al., 2012).

$$t_r = \frac{V}{Q} \quad (7.6)$$

Where, V is the vessel volume and Q is volumetric flow.

6.4.2 DEOXO unit

The sizing of the DEOXO unit can be determined by considering the pressure drop across the reactor bed and the superficial gas velocity. The Ergun equation is a fundamental formula used to calculate the pressure drop in a packed bed of particles and it can be expressed as following:

$$\frac{\Delta P_b}{H_b} = f_m \frac{\rho v^2}{d_p} \left(\frac{1 - \varepsilon_b}{\varepsilon_b} \right) \quad (7.7)$$

Where,

ΔP_b pressure drop across the bed (Pa)

H_b bed heigh (m)

f_m modified coefficient of friction

ε_b bed voidage

μ fluid's dynamic viscosity (Pa s)

v fluid's superficial velocity (m/s)

d_p catalyst particle's diameter (m)

ρ fluid's density (kg/m³)

Modified coefficient of friction can be expressed as following:

$$f_m = a_E + b_E \left(\frac{1 - \varepsilon_b}{R_e} \right) \quad (7.8)$$

Where R_e is Reynolds number and a and b are coefficient values proposed by Ergun $a = 1.75$ and $b = 150$.

When the superficial gas velocity and flow rate are known, the necessary cross-sectional area of the reactor can be determined as follows:

$$v = \frac{Q}{A} \quad (7.9)$$

$$V_{catalyst} = (1 - \varepsilon_b) V_{reactor} \quad (7.10)$$

Where Q is feed flowrate, v is superficial gas velocity, and $V_{catalyst}$ is volume of catalyst and $V_{reactor}$ is reactor volume.

7 Results

7.1 Pressure and temperature influence on AEL system

To evaluate how temperature and pressure impact alkaline electrolysis, electrochemical equations have been employed to forecast the performance of AEL stack across various operating conditions, specifically pressure and temperature in our case. The equations proposed in section (3.4), notably (Eq. (3.11)) and (Eq. (3.26)), enable the determination of the polarization curve and Faraday efficiency as a function of current. Table 11 summarizes the coefficients regarded for the electrochemical model of AEL.

Table 11 Model and simulation variable coefficients

Model	Coefficient	Value	Unit	References
Polarization curve	α_1	0.8	$\Omega \text{ cm}^2$	(Sakas et al., 2021)
	α_2	-0.00763	$(\Omega \text{ cm}^2)/^\circ\text{C}$	(Sakas et al., 2021)
	s	0.1795	V	(Sakas et al., 2021)
	β_1	20	cm^2/A	(Sakas et al., 2021)
	β_2	0.1	$(\text{cm}^2 \text{ }^\circ\text{C})/\text{A}$	(Sakas et al., 2021)
	β_3	3.5e5	$(\text{cm}^2 \text{ }^\circ\text{C}^2)/\text{A}$	(Sakas et al., 2021)
	d_1	-3.12996	$\Omega \text{ cm}^2$	(Sánchez et al., 2019)
	d_2	4.47e-7	$(\Omega \text{ cm}^2)/\text{bar}$	(Sánchez et al., 2019)
Faraday efficiency	f_{11}	478646	A^2/m^4	(Sánchez et al., 2019)
	f_{12}	-2953	$\text{A}^2/(\text{m}^4 \text{ }^\circ\text{C})$	(Sánchez et al., 2019)
	f_{21}	1.0396	-	(Sánchez et al., 2019)
	f_{22}	-0.0021	$1/^\circ\text{C}$	(Sánchez et al., 2019)

7.1.1 Temperature influence on stack performance

Temperature effect on stack performance was investigated using Aspen Plus and excel as it was mentioned before. In the figures, all parameters remain constant except temperature, which is varied to observe its impact on the AEL system. Fig 17a depicts the polarization curve of AEL stack at different temperatures. Based on the results, cell voltage increases with current density and decreases when temperature is increased from 60 °C to 150 °C. Fig 17b illustrates the correlation between stack power and current density. According to the model, the stack power increases with an increase in current density and decreases with an increase in temperature as it can be seen in the model. The reduction of stack power when temperature increases can be explained using polarization curve (Fig 17a). When cell voltage decreases, it means that less electrical potential is required to drive the electrochemical reaction within electrolyzer. This reduction in voltage directly affects the overall power output of the stack. This can also be explained by the power equation, where power is equal to cell voltage (V) times current (I).

Fig 17c displays the hydrogen production rate at various temperatures. Hydrogen production rate usually increases with current density, but the model shows us that there is a slightly decrease in H₂ production rate when temperature increases. The reason behind this is that a rise in temperature reduces resistance, and increases parasitic current losses, which results in lower faraday efficiencies (Sánchez et al., 2019). When faraday efficiencies decrease, hydrogen production rate decreases too.

Fig 17d shows the variations in stack efficiency as the current density increases from 10 to 500 A/m² across temperatures ranging from 60 °C to 150 °C. When current density increases, stack efficiency decreases slightly and stays the same most of the time. As temperature increases from 60 °C to 150 °C, stack efficiency increases from 69 % to 85 %. This is because an increase in temperature enhances electrolyzer stack efficiency by accelerating reaction kinetics, reducing overpotential, improving ionic conductivity, favorably shifting reaction equilibria, and facilitating effective heat management.

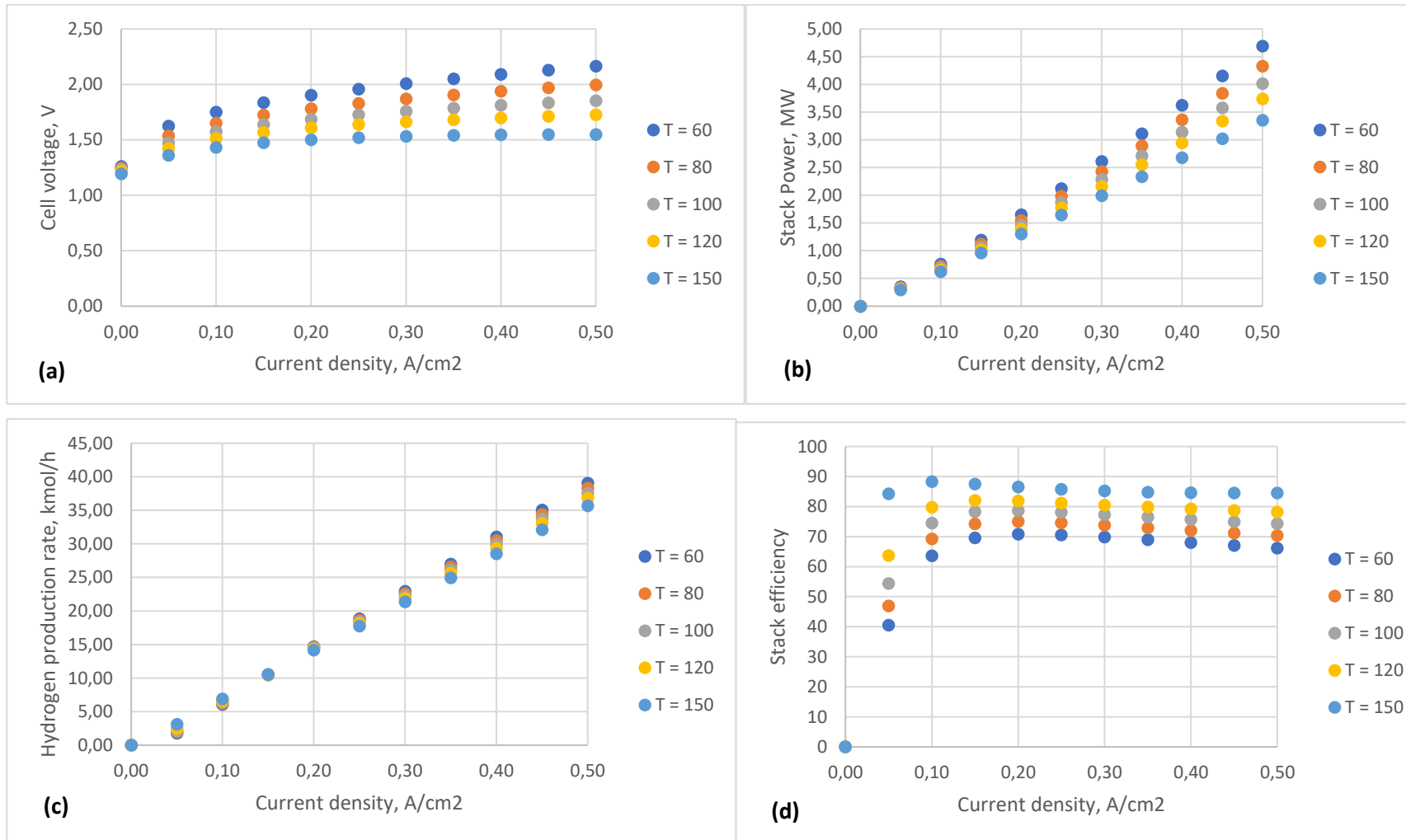


Figure 17 AEL stack performance with various temperatures at 16 bars: a) Polarization curve; b) required stack power; c) Hydrogen flow rate; d) Stack efficiency.

Figure 18 provide an illustration of the relationship between energy consumption (kWh/kg H₂), current density (A/cm²) across a range of operating temperatures. The graph shows us that energy consumption decreases with increasing temperature, showcasing efficiency improvement when using high temperature. By higher temperature, activation energy decreases, which results in faster reaction kinetics, thus decreasing cell voltage and energy consumption.

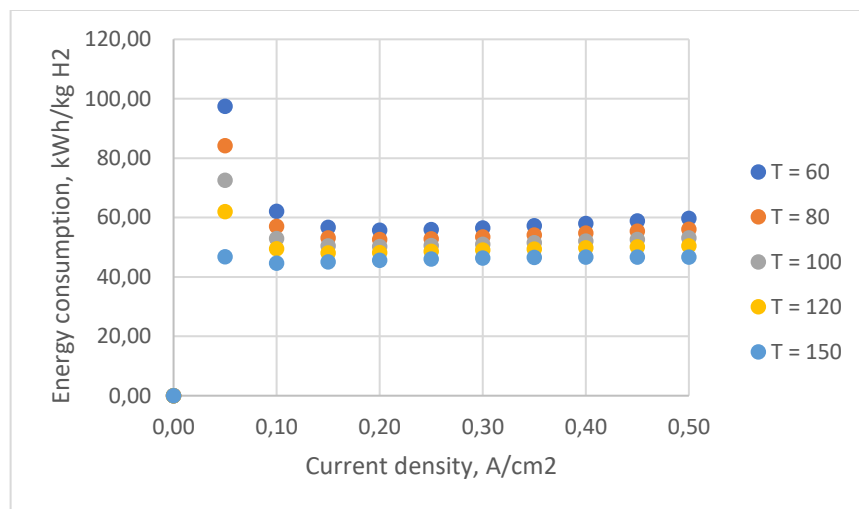


Figure 18 Influence of temperature on energy consumption

Figure 19 shows the variation of the system efficiency with different temperature. As observed, as temperature rises, system efficiency also increases. This is due to the same reason we stated while explaining energy consumption reduction when increasing temperature. Higher temperature enhances the ionic conductivity of the electrolyte and decrease the cell voltage leading to more efficient hydrogen production. When comparing Fig. 19 and Fig. 17d, it can be observed that, system energy is lower than stack efficiency with different temperatures. This is because, in system efficiency calculation, auxiliary power consumption was considered, which decreased slightly the system efficiency. It must be noted also that stack efficiency and system efficiency were calculated using higher heating value (HHV) instead of lower heating value (LHV). This is because HHV accounts for the total energy content of hydrogen, including the latent heat of vaporization of water produced during the reaction.

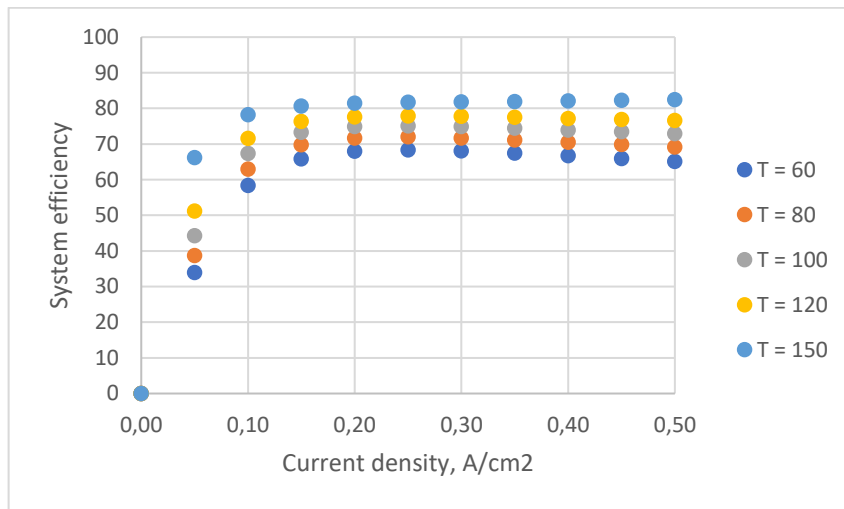


Figure 19 System efficiency with various temperatures

Figure 20 depicts how voltage efficiency changes with varying current density and temperatures. The graph shows that voltage efficiency generally decreases as current density increases, which is expected due to increased overpotentials and resistive losses at higher current densities. It can also be seen that with higher temperature, voltage efficiency increases. The enhanced performance can be attributed to upgraded reaction kinetics and reduced activation energy, which lower the overall cell voltage.

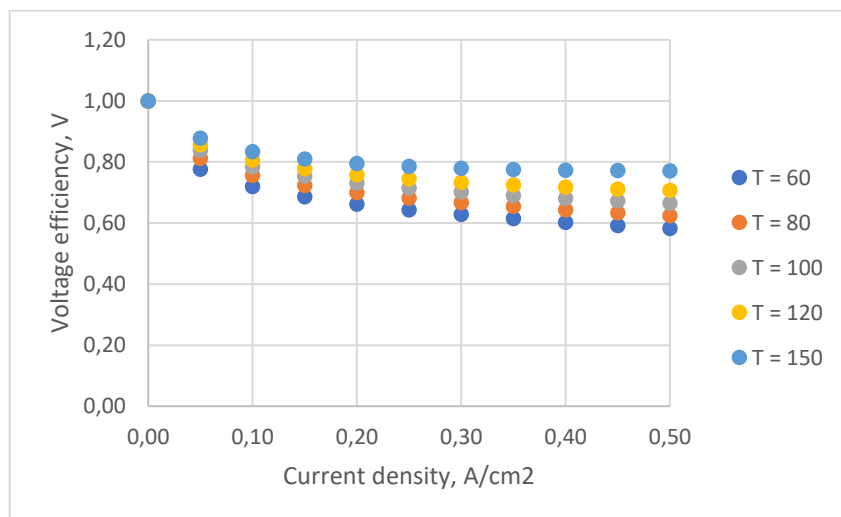


Figure 20 Voltage efficiency at different temperatures

Table 12 summarizes the effect of high temperature on key variables in alkaline electrolysis. The table demonstrates that increasing the operating temperature in alkaline electrolysis significantly enhances efficiency and reduces energy consumption. Higher temperature improves cell voltage, reduces stack power requirements, and enhances both voltage and system efficiencies. These improvements are crucial for making hydrogen production more cost-effective and sustainable.

Table 12 Key performance indicators for AEL at different temperatures with current density of nominal point of 3500 A/m²

Parameter	Temperature				
	60 °C	80 °C	100 °C	120 °C	150 °C
Current density (A/m ²)	3500	3500	3500	3500	3500
Cell voltage (V)	2.09	1.91	1.79	1.68	1.54
Stack power (MW)	3.11	2.89	2.71	2.55	2.34
Hydrogen production rate (kmol/h)	26.99	26.54	26.09	25.63	24.93
Energy consumption (kWh/kg H ₂)	57.20	54.05	51.54	49.40	46.49
Voltage efficiency (%)	61	65	69	72	78
Stack efficiency (%)	69	73	76	80	85
System efficiency (%)	67	71	74	77	82

The solubility of gases in liquid decreases with increasing temperature. Figure 21 clearly demonstrates increasing temperature in AEL leads to a significant reduction in the impurity concentrations of H₂ in O₂ (HTO) and O₂ in H₂ (OTH). This improvement is primarily due to enhanced gas bubble behavior, improved electrolyte conductivity, decreased viscosity, and reduced overpotentials at higher temperatures. These factors contribute to higher purity of the produced gases.

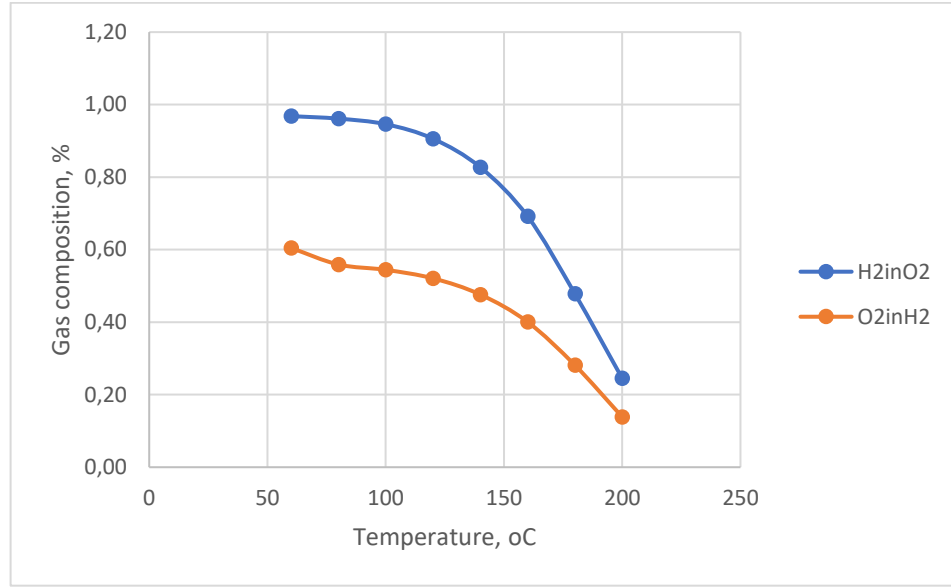


Figure 21 Hydrogen in oxygen and oxygen in hydrogen stream with different temperature.

7.1.2 Pressure influence on stack performance

To assess the influence of pressure fluctuations on AEL system's performance, the developed AEL system model in this study underwent simulation at pressures ranging from 1 to 25. The Nernst equation (Eq. (3.11)) we used to assess the effect of high temperature on AEL system cannot be used with pressure because even though it is also pressure dependent, other variable such as standard equilibrium potential equation (E_{rev}^0) (Eq. (3.12)) and the water activity of the KOH salute ($\alpha_{H_2O,KOH}$) equation (Eq. 3.17)) are only dependent on temperature and since temperature is constant, the results would be wrong. Due to this reason, a polarization equation proposed by Ulleberg (Sánchez et al., 2019) was used to determine the effect of high pressure on AEL system. Concentration overpotentials are not considered in the following equation, mainly because they occur at very high current densities.

$$E_{cell} = E_{rev} + [(a_1 + d_1)] + a_2T + d_2p + s \log \left[\left(\beta_1 + \frac{\beta_2}{T} + \frac{\beta_3}{T^2} \right) i + 1 \right] \quad (8.1)$$

Where, a_1 , a_2 , d_1 , d_2 , β_1 , β_2 , β_3 , s are coefficients mentioned in Table 11, i is current density, E_{rev} is reversible voltage, T is operating temperature and p is operating pressure.

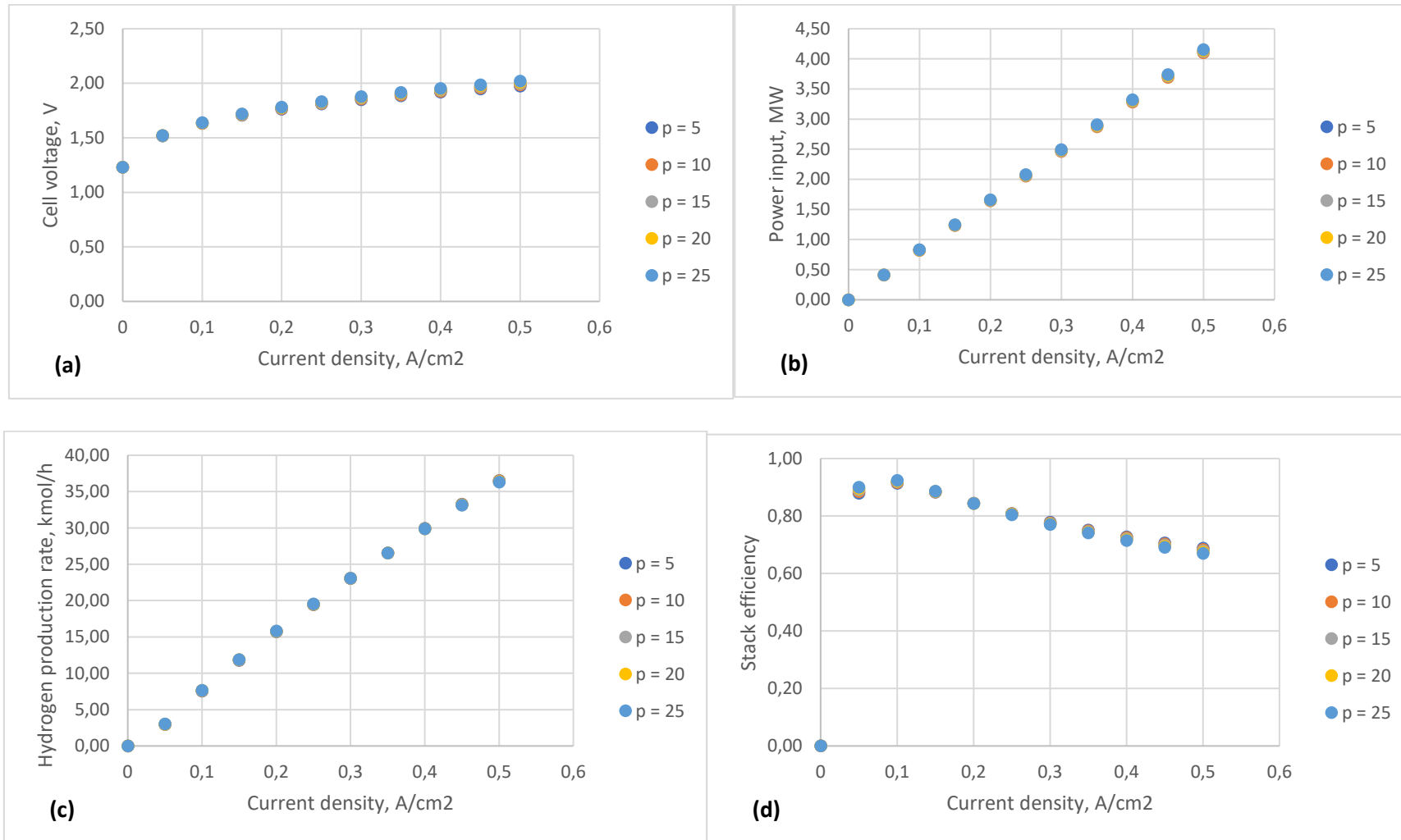


Figure 22 The impact of temperature on the performance of the AEL stack at 16 bars: a) Polarization curve; b) required stack power; c) Hydrogen flow rate; d) Stack efficiency.

Fig 22a shows the polarization curve with different pressures. As it was seen in temperature effect on AEL system, cell voltage tends to increase with increasing of current density. Unlike high temperature, which decreases cell voltage, Fig 22a shows that as pressure increases, cell voltage increases also slightly. This is because high temperature usually increases solubility of gases in the electrolyte, which also raises the overpotential required for gas evolution. Fig 22b shows the power required by AEL stack at different pressures. The graph shows that power increases with current density but stays the same as pressure increases up to 3500 A/m² and starts to increase slightly from 3500 A/m² to 5000 A/m² current density.

Fig 22c illustrates the connection between hydrogen production rate, current density, and pressure. The graph shows that the effect of pressure on hydrogen production rate is so small, thus it can be considered negligible. Fig 22d illustrates a decrease in stack efficiency with increasing current density. Additionally, it indicates that with rising pressure, stack efficiency remains constant until current density of 3000 A/m², whereas after pressure increase decreases stack efficiency slightly as evidenced.

Fig 23 shows that system efficiency decreases with current density. Across the different pressure levels (5 to 25 bar), the efficiency trends remain similar, implying that pressure has a less pronounced effect on system efficiency compared to current density.

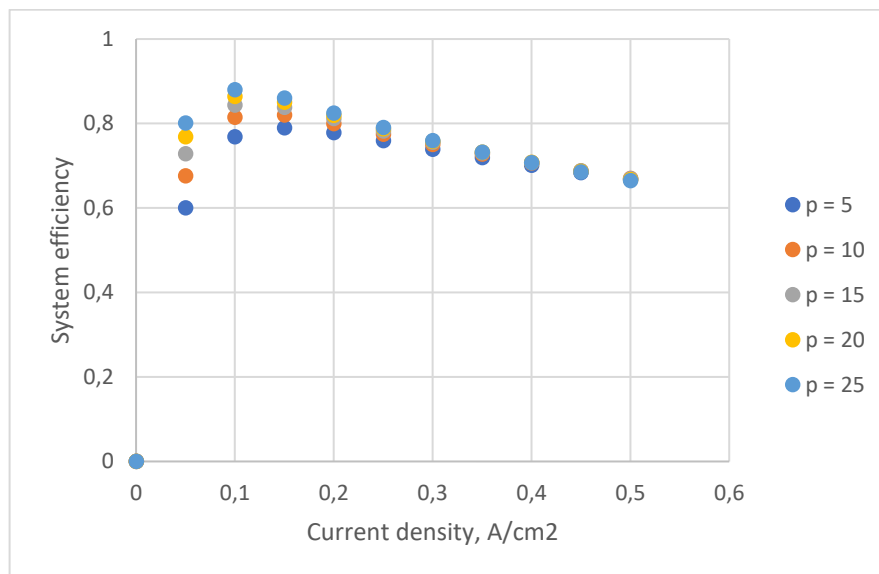


Figure 23 System efficiency with different pressures

The peak system efficiency is observed at a current density around 1000 A/m². Here, efficiency slightly surpasses 0.8 (80%) for all pressure levels, suggesting an optimal operating point where the electrolysis system performs most efficiently. As the current density increases beyond 1000 A/m², a gradual decline in system efficiency is evident. At current densities above 2000 A/m², efficiency drops more noticeably, converging towards approximately 0.6 (60%) at the highest current densities tested (5000 A/m²).

Figure 24 illustrates the relationship between pressure and gas composition in alkaline electrolysis providing a crucial understanding of how pressure affects gas purity. The graph presents a clear linear relationship between pressure (ranging from 0 to 50 bar) and gas composition. This linear increase suggests that higher pressures exacerbate the permeation of hydrogen into the oxygen stream, because of the higher diffusion rate and solubility of hydrogen at elevated pressures. For alkaline electrolysis, it is crucial to maintain gas purity below the explosive limit. Alkaline electrolyzers (AEL) are particularly vulnerable to safety accidents when the hydrogen-threshold oxygen (HTO) concentration ranges from 3.8% to 95.4%. Most AEL systems perform a safety shutdown when HTO reaches 50% of the lower limit value, which is 3.8%. This means the system must be stopped if HTO exceeds 1.9%. According to the graph, we remain below the safety limit at 30 bars. HTO not only poses safety risks but also reduces Faraday efficiency (Hu et al., 2022). Regarding the oxygen-threshold hydrogen (OTH) limit, the graph indicates that pressure can be increased up to 50 bars without reaching the safety limit.

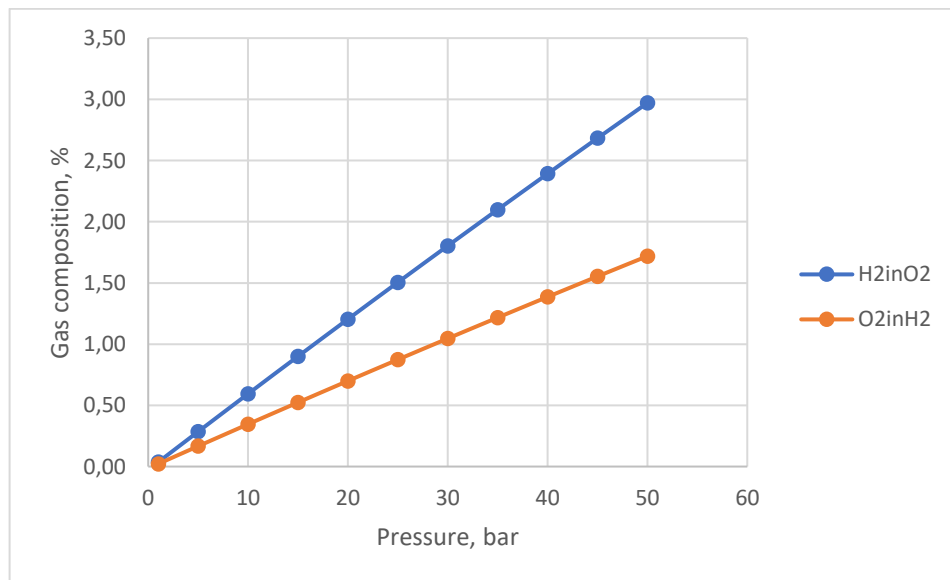


Figure 24 Pressure effect on hydrogen in oxygen and oxygen in hydrogen stream

7.2 Development of electrolysis cost model

7.2.1 Estimation of investment capital cost

The cost estimation for the alkaline electrolysis process option relied on the simulation results. Aspen Economic Evaluation provided estimates for the major equipment costs and utility costs, which were then utilized in the cost estimation calculations. To ensure the precision in the results, the costs derived from Aspen Plus Economic Analysis (APEA) are further adjusted by multiplying them with a material factor (f_m). The following table provides typical values of the material factor for commonly used engineering alloys.

Table 13 Material factor for different alloys (Sinnott & Towler, 2015)

Material	f_m
Carbon steel	1.0
Stainless steel (304)	1.3
Aluminum and bronze	1.07
Stainless steel (316)	1.3
Cast steel	1.1
Stainless steel (321)	1.5
Monel	1.65
Hastelloy C	1.55
Nickel and Inconel	1.7

In the context of material considerations, the default assumption in the analysis is most of the equipment in the process is constructed from carbon steel ($f_m = 1.0$). The alkaline electrolyzer (AE), hydrogen and oxygen separators and heat transfers are constructed from nickel coated material. However, due to limited information, the material factor for the nickel coating was not determined. The equipment and installation costs for each component are detailed in Table 14. The cost of the AE listed in Table 14 pertains only to the electrolyzer stack shell and does not include components such as the electrodes and diaphragm.

Table 14 The cost for 2.84 MW alkaline electrolyzer obtained from Aspen plus economics.

Equipment type and ID	Specification	Purchase cost (€)	Installed cost (€)	Material factor	Corrected cost (€)
Compressors					
COMPRES	H ₂ (16 bar to 30 bar)	461288	549884	1.0	549884
COMPRES2	H ₂ (30 bar to 50 bar)	459540	549516	1.0	549516
Pumps					
	Deionized H ₂ O to O ₂ separator				
PUMP1		18860	48944	1.0	48944
PUMP2		8648	57316	1.0	57316
PUMP3		8556	57224	1.0	57224
	Cooling H ₂ O to heat exchanger				
PUMP4		5084	31648	1.0	31648
Reactors					
AE	Drying H ₂	219236	413908	-	-
DEOXO	H ₂ O formation	40940	209484	1.0	209484
DEOXO2	H ₂ O formation	81512	331200	1.0	331200
Pressure vessels					
	Separating H ₂ from electrolyte				
FLASH1		40388	175168	-	-
	Separating O ₂ from electrolyte				
FLASH2		40388	175168	-	-
DRYER		22448	118588	1.0	118588
DRYER		22448	118588	1.0	118588
Heat exchangers					
HE1		13892	78476	-	-
HE2		13892	78476	-	-
AIRCOOL		9660	60628	1.0	60628
COOLER		12604	76452	1.0	76452
COOLER2		12696	79212	1.0	79212
Total		1411188	2878680	13	2878680

The compressors cost depends on the process pressure. The compressors costs and power consumption were calculated using Aspen Plus at various pressures. The model compared the use of two compressors versus one compressor to assess differences in costs and power

consumption. In commercial alkaline electrolysis, multiple compressors are used to prevent the outlet temperature from exceeding the limit, making a single compressor impractical.

Table 15 presents the compressor costs and power consumption at different process pressures. In the Aspen model, hydrogen undergoes compression to 50 bar. Through a multi-compressor arrangement, the hydrogen is initially compressed to 30 bar in the first compressor and subsequently to 50 bar in the second compressor. The results indicate that at process pressure of 15 bar, the compressor cost is 0.83 M€ when compressing from 15 bar to 50 bar, 0.52 M€ from 15 bar to 30 bar, and 0.42 M€ (from 30 bar to 50 bar). The corresponding power consumption is 55 kW, 26 kW, and 21 kW, respectively. The table demonstrates that using two compressors generally reduces both the equipment cost and power consumption compared to using one compressor, particularly at lower process pressures. This efficiency arises because multi-compressor setups better manage temperature and pressure stages, preventing excessive energy use and reducing equipment stress.

Table 15 Compressor costs at different operational pressures

Process pressure	AEL with one compressor		AEL with two compressors			
	Equipment cost, M€	Power, kW	Equipment cost, M€	50 bar cost, M€	30 bar Power (kW)	50 bar Power (kW)
	50 bar	50 bar	30 bar	50 bar	30 bar	50 bar
1 bar	1.57	269	1.1	0.45	187	21
5 bar	1.20	124	0.63	0.45	76	21
10 bar	0.98	78	0.52	0.45	42	21
15 bar	0.84	55	0.51	0.45	26	21
20 bar	0.62	40	0.46	0.45	19	21
25 bar	0.59	29	0.41	0.45	14	21
30 bar	0.54	21	-	-	-	-
35 bar	0.52	14	-	-	-	-
40 bar	0.51	9	-	-	-	-
45 bar	0.47	4	-	-	-	-
49 bar	0.32	0	-	-	-	-

Table 16 presents key parameters and assumptions used for calculating the operating costs associated with Alkaline Electrolysis systems. The cost of water, potassium hydroxide and service and maintenance were calculated using values from (Jang et al., 2022) literature review on 1 MW Alkaline electrolysis process. It is assumed that the plant operates in three shifts, with each shift requiring one operator and one shift supervisor. Annually, the salary expenses amount to 120,000 euros for the three operators and 180,000 euros for the three shift supervisors. Other operating costs include overhead expenses that are not listed in the following table such as insurance and plant taxes.

Table 16 Cost factors and value of a 2.78 MW AEL

Items	Value	Unit	Reference
Interest rate	8	%	
Interest time	20	years	
Operating hour	8000	hours/a	
Electric cost	50	€/MWh	
Labor	40000	€, full time	
Shift supervisor	60000	€, full time	
KOH	2.29	€/kg	(Jang et al., 2022)
H ₂ O	0.01	€/kg	(Jang et al., 2022)
Service and Maintenance	2-3	% of CAPEX	(Jang et al., 2022)
Other operating cost	1	% of CAPEX	(Jang et al., 2022)

Table 17 provides a comprehensive breakdown of the operating and capital costs for two different sizes of Alkaline Electrolysis (AEL) systems: a 2.78 MW alkaline electrolysis operating at 80 °C and 16 bar simulated in this work and a 1 MW alkaline electrolysis operating at 80 °C and 30 bar from a study by (Jang et al., 2022).

Based on Jang et al. (Jang et al., 2022) article, the cost of the alkaline electrolysis process was estimated to be 1.5 M€/MW, equaling to 4.17 M€ for 2.78 MW. In the calculations, the cost of balance-of-plant equipment was determined using Aspen Plus cost estimations. However, the electrolyzer cost was assumed to be 1.8 M€, representing 43% of the total investment cost for the electrolysis process. OSBL and contingency costs were assumed to be the same as for a 1 MW system, as the compressor size has minimal impact on OSBL

costs. The costs for other balance of plant components were calculated assuming a linear increase based on the 1 MW process.

The 2.78 MW AEL system, while having substantially higher capital and operating costs than the 1 MW AEL, also offers a significantly higher hydrogen production rate. This indicates economies of scale, where the larger system, despite higher upfront and running costs, is more efficient in terms of hydrogen output. The higher production rate justifies the larger investment, especially when considering the increased hydrogen output, which can potentially lead to lower hydrogen costs per unit over time.

Table 17 Comparison of a 2.78 MW AEL at 80 °C, 15 bar and 1 MW industrial AEL from (Jang et al., 2022) article.

		2.78 MW AEL	1MW AEL
Items		Value	Value
Capital cost (\$)	Stack cost	1800000	340000
	Water circulation	130000	87082
	H ₂ processing	1470000	83880
	Cooling	80000	28678
	Other BoPs	567746	204225
	Total ISBL	4047746	743865
	OSBL, 10 %	74386	74386
	Engineering cost, 10%	34800	7438
	Contingency cost, 10%	82569	82569
	Total investment cost	4239501	908259
Operating cost (\$/year)			
	Electricity	1130000	292000
	Labor	120000	36575
	Supervisor	180000	-
	KOH	26311	480
	H ₂ O	49904	8648
	Service and maintenance	84982	14877
	Other operating cost	42491	7439
	Total	1633687	360020
H ₂ production rate	(kg H ₂ / year)	552000	86488

ACCR (Annual Capital Charge Rate) was used to convert total capital investment cost into annualized capital cost, considering both the interest rate and interest time. To calculate ACCR, you can use the following formula, which is derived from the annuity formula for capital recovery:

$$ACCR = \frac{r(1+r)^n}{(1+r)^n - 1} \quad (7.1)$$

Where,

r is annual interest rate

n is plant's lifetime in years.

The calculated ACCR was 0.1022, which means that the annual capital charge rate for the investment is 10.22% of the total capital investment. This rate accounts for both the interest cost of capital and the depreciation over the 20-year lifespan of the plant.

Table 18 provides a detailed analysis of the CAPEX, OPEX, and overall costs associated with an Alkaline Electrolysis (AEL) system operating at different pressure levels. It also includes system energy consumption (SEC), hydrogen production capacity, and cost per ton of hydrogen. The yearly CAPEX is calculated by multiplying the ACCR by the total CAPEX. The cost per kg of hydrogen can be calculated as follows:

$$\text{Cost per kg H}_2 = \frac{\text{Total annual cost}}{\text{Annual H}_2 \text{ production cost}} \quad (7.2)$$

Table 18 illustrates the impact of compressor costs at different pressures on CAPEX, OPEX, and hydrogen production costs. As the process pressure increases, compressor costs decrease, resulting in lower CAPEX at higher pressures. At a process pressure of 1 bar, CAPEX is at its highest due to the cost of the compressors, resulting in increased hydrogen production costs. At a process pressure of 30 bar, the system requires only one compressor to compress hydrogen to 50 bar, leading to a lower overall CAPEX and reduced hydrogen costs.

Table 18 Hydrogen production costs of alkaline electrolysis calculated for 2.78 MW unit operating at 80 °C with various pressure.

Pressure	CAPEX (M€)	CAPEX (M€/a)	OPEX (M€/a)	Total (M€/a)	SEC (MWh/t H ₂)	Capacity (t H ₂ /a)	Cost, (€/t H ₂)
1	4.930	0.502	1.194	1.697	52.53	423.4	4007.2
5	4.308	0.439	1.150	1.589	53.25	417.7	3804.0
10	4.161	0.424	1.136	1.560	53.74	413.8	3770.1
15	4.149	0.423	1.130	1.553	54.01	411.8	3770.5
20	4.076	0.415	1.127	1.542	54.2	410.3	3758.7
25	4.015	0.409	1.125	1.534	54.43	408.6	3754.5
30	2.867	0.292	1.120	1.412	54.47	408.3	3457.3

It should be noted that these results were calculated based on varying costs of only the compressors at different pressures. The costs of pumps and other AEL equipment were kept constant at an operating condition of 80°C and 16 bar due to limited time of resources.

7.2.2 Variable costs and revenue

The revenue and variable cost of alkaline electrolysis are presented in Table 19. The hydrogen production rate of AEL is 552 t/y, and the oxygen production rate is 4384 t/y. Based on the unit price of hydrogen, approximately 2.3 million euros in revenue is generated. The hydrogen production cost was calculated as \$3.77 per kg, given that wind electricity, a renewable energy source, is used. Electricity is assumed to cost \$50 per MWh, while the prices of water and KOH are \$0.01 per kg H₂O and \$2.92 per kg KOH, respectively. According to the calculations, the yearly electricity consumption for the electrolyzer is 22.24 GWh (2.78 MWh), while the electricity consumption for other auxiliary components is 0.48 GWh (60 kWh) per year.

Table 19 Variable costs and revenue of the AEL process at operating condition of 80 °C and 16 bar.

	Units	Unit per year	Price \$/Unit	M\$ per year
Water	t	4990	10	0.049
KOH	t	9.01	2920	0.026
Electricity	GWh	22.24	50000	1.112
Utilities	GWh	0.48	50000	0.024
Main product revenue				
Hydrogen	t	552	3770.5	2.08
Oxygen	t	4384	54	0.237
Total variable costs	-	-	-	1.212
Revenue	-	-	-	2.318

8 Conclusions

In this thesis, a comprehensive Aspen Plus model of AEL plant has been developed, incorporating both the stack and the balance of plant using verified industrial data. The industrial facility is strategically designed to operate for 333,3 days per year, corresponding to 8000 hours annually. Economic analysis was conducted to investigate the effect of pressure on alkaline electrolysis equipment cost.

The production cost of 1 kg of hydrogen using a 2.78 MW plant at process pressures of 5, 10, 15, 20, 25, and 30 bar was calculated to be 3.804 €/kg H₂, 3.770 €/kg H₂, 3.770 €/kg H₂, 3.758 €/kg H₂, 3.754 €/kg H₂, and 3.457 €/kg H₂, respectively. Due to time constraints, the calculations focused only on the impact of compressor costs on the capital expenditure (CAPEX) at different process pressures, rather than considering the costs of all process equipment at various pressures. To fully understand the effect of pressure on CAPEX, process capacity, and hydrogen production cost, the costs of all equipment at different pressures should be considered. This comprehensive analysis was not feasible within the timeframe of this thesis, but a subsequent study will be conducted to thoroughly explore the influence of pressure on AEL costs.

The study also investigated the effects of pressure and temperature on the I-U curve, hydrogen flow rate, stack power, and energy efficiency of an advanced AEL system. Simulations were performed with temperatures ranging from 60°C to 150°C and pressures from 1 bar to 25 bar. The results revealed that pressure does not significantly impact the hydrogen flow rate, cell voltage, stack power, or system efficiency. However, pressure does affect the gas composition within the electrolyzer, with higher pressures significantly increasing the hydrogen-to-oxygen (HTO) ratio, while the oxygen-to-hydrogen (OTH) ratio increases but slowly compared to HTO. According to the results, HTO safety limit of 2 % is met at process pressure of 33 bars, while OTH remains below the safety limit at process pressure of 50 bar.

The analysis indicates that operating the advanced alkaline electrolysis system at higher temperatures (120°C and 150°C) improves the overall electrochemical efficiency. This is evidenced by the lower cell voltages and slightly lower stack power requirements at higher temperatures, which imply reduced energy losses and higher energy efficiency. However,

the hydrogen production rate remains largely unaffected by temperature, indicating that current density is the dominant factor in determining production rates. Therefore, optimizing the operating temperature to higher levels can enhance energy efficiency without compromising hydrogen output.

9 References

Adolphsen, J.Q., 2018. Development and characterization of high temperature and-pressure alkaline electrolysis cells (HTP-AECs). Pp. 15-19. Available online: https://backend.orbit.dtu.dk/ws/portalfiles/portal/184485934/JensQAdolphsen_PhD_thesis_August_2018.pdf

Allebrod, F., Chatzichristodoulou, C. and Mogensen, M.B., 2013. Alkaline electrolysis cell at high temperature and pressure of 250 C and 42 bar. *Journal of Power Sources*, 229, pp.22-31.

Amores, E., Sánchez, M., Rojas, N. and Sánchez-Molina, M., 2021. Renewable hydrogen production by water electrolysis. In *Sustainable fuel technologies handbook* (pp. 271-313). Academic Press. Available online: https://mdpi-res.com/processes/processes-08-00248/article_deploy/processes-08-00248-v2.pdf?version=1582684442

Azuan, M., Yahaya, N.Z., Melinda, A. and Umar, M.W., 2019. Effect of Temperature on Performance of Advanced Alkaline Electrolyser. *Science International (Lahore)*, pp.757-762. Available online: <http://www.sci-int.com/pdf/637054513794717651.pdf>

Brauns, J. and Turek, T., 2020. Alkaline water electrolysis powered by renewable energy: A review. *Processes*, 8(2), p.248. Available online: https://mdpi-res.com/processes/processes-08-00248/article_deploy/processes-08-00248-v2.pdf?version=1582684442

Buttler, A. and Spliethoff, H., 2018. Current status of water electrolysis for energy storage, grid balancing and sector coupling via power-to-gas and power-to-liquids: A review. *Renewable and Sustainable Energy Reviews*, 82, pp.2440-2454.

Chatenet, M., Pollet, B.G., Dekel, D.R., Dionigi, F., Deseure, J., Millet, P., Braatz, R.D., Bazant, M.Z., Eikerling, M., Staffell, I. and Balcombe, P., 2022. Water electrolysis: from textbook knowledge to the latest scientific strategies and industrial developments. *Chemical Society Reviews*, 51(11), pp.4583-4762. Available online: <https://pubs.rsc.org/en/content/articlepdf/2022/cs/d0cs01079k>

Dayama, P.O., 2021. A Comparative Study of Electrodes and Membranes for Anion Exchange Membrane Water Electrolysis Systems. M.Sc. thesis, KTH, Sweden. Available online: <https://kth.diva-portal.org/smash/get/diva2:1588565/FULLTEXT01.pdf>

Perrin, O., Pinto, J.M., Kuzmanovic, A., Singhraj, H.E., Law-Kam, C., Lim, P., Mokrane, K., 2021. Fueling the future of mobility: hydrogen electrolyzers. *Monitor Deloitte*. Pp. 4-5.

Available online: <https://www2.deloitte.com/content/dam/Deloitte/jp/Documents/global-business-support/jp-gbs-fueling-the-future-of-mobility-hydrogen-electrolyzers.pdf>

Đurovič, M., Hnát, J. and Bouzek, K., 2021. Electrocatalysts for the hydrogen evolution reaction in alkaline and neutral media. A comparative review. *Journal of Power Sources*, 493, p.229708.

Ebbesen, S.D., Jensen, S.H., Hauch, A. and Mogensen, M.B., 2014. High temperature electrolysis in alkaline cells, solid proton conducting cells, and solid oxide cells. *Chemical reviews*, 114(21), pp.10697-10734. Available online: <https://pubs-acsc-org.ezproxy.cc.lut.fi/doi/epdf/10.1021/cr5000865>

Faid, A.Y. and Sunde, S., 2022. Anion exchange membrane water electrolysis from catalyst design to the membrane electrode assembly. *Energy technology*, 10(9), p.2200506. Available online: <https://onlinelibrary-wiley-com.ezproxy.cc.lut.fi/doi/epdf/10.1002/ente.202200506>

Ganley, J.C., 2009. High temperature and pressure alkaline electrolysis. *International journal of hydrogen energy*, 34(9), pp.3604-3611.

Godula-Jopek, A., 2015. *Hydrogen production: by electrolysis*. John Wiley & Sons. Pp. 117–137.

Hauch, A., Ebbesen, S.D., Jensen, S.H. and Mogensen, M., 2008. Highly efficient high temperature electrolysis. *Journal of Materials Chemistry*, 18(20), pp.2331-2340. Available online: <https://pubs-rsc-org.ezproxy.cc.lut.fi/en/content/articlepdf/2008/jm/b718822f?page=search>

Haug, P., Koj, M. and Turek, T., 2017. Influence of process conditions on gas purity in alkaline water electrolysis. *International Journal of Hydrogen Energy*, 42(15), pp.9406-9418.

Holst, M., Aschbrenner, S., Smolinka, T., Voglstätter, C. and Grimm, G., 2021. Cost forecast for low-temperature electrolysis-technology driven bottom-up prognosis for PEM and alkaline water electrolysis systems. Fraunhofer Institute for Solar Energy Systems ISE: Freiburg, Germany.

Hu, S., Guo, B., Ding, S., Yang, F., Dang, J., Liu, B., Gu, J., Ma, J. and Ouyang, M., 2022. A comprehensive review of alkaline water electrolysis mathematical modeling. *Applied Energy*, 327, p.120099.

Jang, D., Cho, H.S. and Kang, S., 2021. Numerical modeling and analysis of the effect of pressure on the performance of an alkaline water electrolysis system. *Applied energy*, 287, p.116554.

Jang, D., Cho, H.S., Lee, S., Park, M., Kim, S., Park, H. and Kang, S., 2023. Investigation of the operation characteristics and optimization of an alkaline water electrolysis system at high temperature and a high current density. *Journal of Cleaner Production*, 424, p.138862.

Jang, D., Kim, J., Kim, D., Han, W.B. and Kang, S., 2022. Techno-economic analysis and Monte Carlo simulation of green hydrogen production technology through various water electrolysis technologies. *Energy Conversion and Management*, 258, p.115499.

KEMI., 2022. Vedyn mahdollisuudet Kemille Teknologiaselvitys loppuraportti.

Kiesilä, P., 2021. Vetytalous ja vedyn tuotanto eri teknologioilla: Teknistaloudellinen vertailu Bachelor's thesis, Tampereen yliopisto. Saatavilla: <https://trepo.tuni.fi/bitstream/handle/10024/133884/Kiesil%C3%A4Pyry.pdf>

Koj, M., Gimpel, T., Schade, W. and Turek, T., 2019. Laser structured nickel-iron electrodes for oxygen evolution in alkaline water electrolysis. *International Journal of Hydrogen Energy*, 44(25), pp.12671-12684.

Koponen, J., 2015. Review of water electrolysis technologies and design of renewable hydrogen production systems. Master thesis, LUT University. Available online: https://lutpub.lut.fi/bitstream/handle/10024/104326/MScThesis_JKK.pdf?sequence=2&isAllowed=y

Krishnan, S., Koning, V., de Groot, M.T., de Groot, A., Mendoza, P.G., Junginger, M. and Kramer, G.J., 2023. Present and future cost of alkaline and PEM electrolyser stacks. *international journal of hydrogen energy*, 48(83), pp.32313-32330.

Kuckshinrichs, W., Ketelaer, T. and Koj, J.C., 2017. Economic analysis of improved alkaline water electrolysis. *Frontiers in Energy Research*, 5, p.1. Available online: <https://juser.fz-juelich.de/record/827015/files/fenrg-05-00001.pdf>

La Camera, F., 2020. Green Hydrogen Cost Reduction: Scaling up Electrolysers to Meet the 1.50C Climate Goal, International Renewable Energy Agency, Abu Dhabi.

Lahtinen, L., 2019. Hydrogen production in small-scale electrolysis units.

Larralde, E. and Ocampo, R., 2011. Selection of gas compressors: part 1. World Pumps, 2011(5), pp.24-28. Available online: <http://csmres.co.uk/cs.public.upd/article-downloads/8Proof-55650.pdf>

Lettenmeier, P., 2021. Efficiency - Electrolysis. SIEMENS Energy. Available online: https://p3.aprimocdn.net/siemensenergy/a00d762d-02bc-4b19-a8c1-b05900db9182/Efficiency-White-paper-pdf_Original%20file.pdf

Leveälahti, R., 2023. Power-to-X-teknikat energia-tuotteiksi. Bachelors thesis, Tampereen yliopisto. Available online: <https://trepo.tuni.fi/bitstream/handle/10024/152297/LevealahtiRea.pdf?sequence=2&isAllowed=y>

Li, W., Tian, H., Ma, L., Wang, Y., Liu, X. and Gao, X., 2022. Low-temperature water electrolysis: fundamentals, progress, and new strategies. Materials Advances, 3(14), pp.5598-5644. Available online: <https://pubs.rsc.org/en/content/articlepdf/2022/ma/d2ma00185c>

Lingkang, J., Nakashima, R.N., Comodi, G. and Frandsen, H.L., 2023. Alkaline electrolysis for green hydrogen production: techno-economic analysis of temperature influence and control. In 36th International Conference on Efficiency, Cost, Optimization, Simulation and Environmental Impact of Energy Systems (pp. 908-919). ECOS. Available online: https://backend.orbit.dtu.dk/ws/portalfiles/portal/333040811/069564_0082open.pdf

Lohmann-Richters, F.P., Renz, S., Lehnert, W., Müller, M. and Carmo, M., 2021. Challenges and opportunities for increased current density in alkaline electrolysis by increasing the operating temperature. Journal of The Electrochemical Society, 168(11), p.114501. Available online: <https://iopscience-iop-org.ezproxy.cc.lut.fi/article/10.1149/1945-7111/ac34cc/pdf>

Mayyas, A. and Mann, M., 2019. Manufacturing competitiveness analysis for hydrogen refueling stations. International Journal of Hydrogen Energy, 44(18), pp.9121-9142. Available online: <https://www.nrel.gov/docs/fy19osti/71304.pdf>

Millet, P., 2015. Fundamentals of water electrolysis. Hydrogen Production: Electrolysis, pp.33-62.

Nami, H., Rizvandi, O.B., Chatzichristodoulou, C., Hendriksen, P.V. and Frandsen, H.L., 2022. Techno-economic analysis of current and emerging electrolysis technologies for green hydrogen production. Energy Conversion and Management, 269, p.116162.

Nguyen, T., Abdin, Z., Holm, T. and Mérida, W., 2019. Grid-connected hydrogen production via large-scale water electrolysis. Energy conversion and management, 200, p.112108.

Parra, D., and Patel, M.K., 2016. Techno-economic implications of the electrolyser technology and size for power-to-gas systems. International Journal of Hydrogen Energy, 41(6), pp.3748-3761.

Phillips, R. and Dunnill, C.W., 2019. Zero gap cell design for alkaline electrolysis. A PHD Thesis, Energy Safety Research Institute, Swansea University Prifysgol Abertawe.

Rajala, V.V., 2022. Elektrolyysitekniikoiden hyötysuhteet vihreän vedyn tuotannossa. Insinöörityö, Vaasan ammattikorkeakoulu. Saatavilla: [https://www.theseus.fi/bitstream/handle/10024/751111/Elektrolyysitekniikoiden%20hy%F6tysuhteet%20vihre%20vedyn%20tuotannossa%20\(1\).pdf?sequence=2](https://www.theseus.fi/bitstream/handle/10024/751111/Elektrolyysitekniikoiden%20hy%F6tysuhteet%20vihre%20vedyn%20tuotannossa%20(1).pdf?sequence=2)

Rashid, M.D., Al Mesfer, M.K., Naseem, H. and Danish, M., 2015. Hydrogen production by water electrolysis: a review of alkaline water electrolysis, PEM water electrolysis and high temperature water electrolysis. International Journal of Engineering and Advanced Technology. Available online: <https://www.ijeat.org/wp-content/uploads/papers/v4i3/C3749024315.pdf>

Sakas, G., Ibáñez-Rioja, A., Ruuskanen, V., Kosonen, A., Ahola, J. and Bergmann, O., 2022. Dynamic energy and mass balance model for an industrial alkaline water electrolyzer plant process. International Journal of Hydrogen Energy, 47(7), pp.4328-4345.

Sánchez, M., Amores, E., Abad, D., Rodríguez, L. and Clemente-Jul, C., 2020. Aspen Plus model of an alkaline electrolysis system for hydrogen production. International journal of hydrogen energy, 45(7), pp.3916-3929.

Santos, D.M., Sequeira, C.A. and Figueiredo, J.L., 2013. Hydrogen production by alkaline water electrolysis. *Química Nova*, 36, pp.1176-1193. Available online: <https://www.scielo.br/j/qn/a/KyQvF9DMHK6ZJXyL5zQNy7N/?format=pdf&lang=en>

Saur, G., 2008. Wind-to-hydrogen project: electrolyzer capital cost study (No. NREL/TP-550-44103). National Renewable Energy Lab.(NREL), Golden, CO (United States). Available online: <https://www.nrel.gov/docs/fy09osti/44103.pdf>

Schmidt, O., Gambhir, A., Staffell, I., Hawkes, A., Nelson, J. and Few, S., 2017. Future cost and performance of water electrolysis: An expert elicitation study. *International journal of hydrogen energy*, 42(52), pp.30470-30492.

Sinnott, R.A.Y., 2014. *Chemical engineering design* (Vol. 6). Elsevier. Available online: <http://doi.org/10.1016/B978-0-08-096659-5.00007-9>

Song, H., Kim, Y. and Yang, H., 2023. Design and Optimization of an Alkaline Electrolysis System for Small-Scale Hydropower Integration. *Energies*, 17(1), p.20.

Tuomivirta, T., 2023. Hydrogen production from renewable resources and hydrogen economy in high school chemistry education. Pro-gradu, University of Eastern Finland. Pp. 7-9. https://erepo.uef.fi/bitstream/handle/123456789/29232/urn_nbn_fi_uef-20230084.pdf?sequence=1&isAllowed=y

Uki, T., Sarda, S.T. and Mathew, T., 2012. Design of gas-liquid separator for complete degassing. *International Journal of Chemical Engineering and Applications*, 3(6), pp.477-480. Available online: <https://ijcea.org/papers/247-W013.pdf>

Ursua, A., Gandia, L.M. and Sanchis, P., 2011. Hydrogen production from water electrolysis: current status and future trends. *Proceedings of the IEEE*, 100(2), pp.410-426. Available online: <https://ieeexplore-ieee.org.ezproxy.cc.lut.fi/stamp/stamp.jsp?tp=&arnumber=5898382>

Viinanen, T., 2023. Alkalielektrolyysin elektrodimateriaalien sähkökemiallinen karakterisointi. Master's thesis, LUT university. Available online: https://lutpub.lut.fi/bitstream/handle/10024/166151/Diplomity%c3%b6_Viinanen_Toni.pdf?sequence=1&isAllowed=y

Vincent, I. and Bessarabov, D., 2018. Low-cost hydrogen production by anion exchange membrane electrolysis: A review. *Renewable and Sustainable Energy Reviews*, 81, pp.1690-1704.

Xu, H., Lattimer, J., Mohan, Y., McCatty, S., Singh, P., Rahman, M.A. and Aphale, A., 2020. High-temperature alkaline water electrolysis. U.S. Department of Energy. (No. DOE-GINER-07644; DOE/DE-EE0007644). Giner, Inc., Newton, MA (United States).

Yakdehige, S.K.D.S., 2017. Design of an Alkaline Electrolysis Stack (Master's thesis, Universitetet i Agder; University of Agder). Available online: <https://core.ac.uk/download/pdf/225893186.pdf>

Yde, L., Kjartansdóttir, C.K. and Allebrod, F., 2013. 2nd Generation alkaline electrolysis. Final report. Århus University Business and Social Science – Centre for Energy Technologies.

Záchenská, J., Jorík, V., Vančo, L., Mičušík, M. and Zemanová, M., 2022. Ni–Fe Cathode Catalyst in Zero-Gap Alkaline Water Electrolysis. *Electrocatalysis*, 13(4), pp.447-456.

Zeng, K. and Zhang, D., 2010. Recent progress in alkaline water electrolysis for hydrogen production and applications. *Progress in energy and combustion science*, 36(3), pp.307-326.

Appendices

Appendix I

Table I Pressure effect on alkaline electrolysis with various temperature at current density of 0.35 A/cm²

	AEL with one compressor		AEL with two compressors			
Process pressure	Equipment cost, \$M	Power, kW	Equipment costs, \$M		Power, kW	
	50 bar	50 bar	30 bar	50 bar	30 bar	50 bar
1 bar	1.71	269	1.2	0.49	187	19
5 bar	1.30	124	0.69	0.49	76	19
10 bar	1.07	78	0.57	0.49	42	19
15 bar	0.91	55	0.56	0.49	26	19
20 bar	0.67	40	0.50	0.49	19	19
25 bar	0.64	29	0.45	0.49	14	19
30 bar	0.59	21	-	-	-	-
35 bar	0.57	14	-	-	-	-
40 bar	0.55	9	-	-	-	-
45 bar	0.51	4	-	-	-	-
49 bar	0.35	0	-	-	-	-

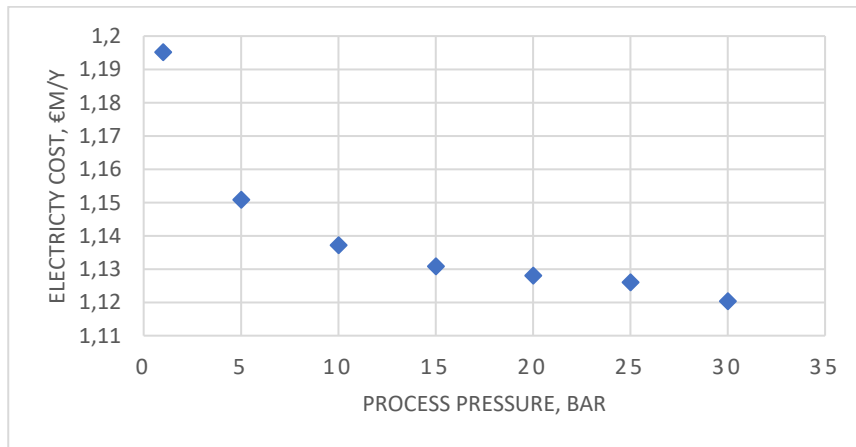
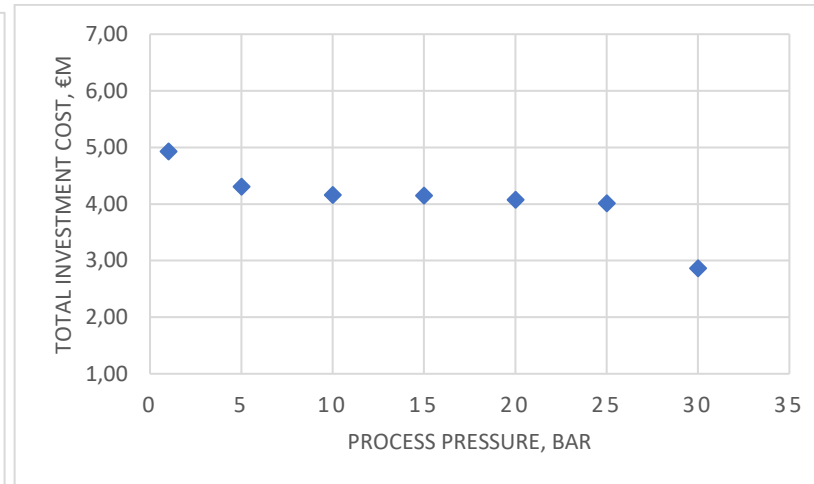
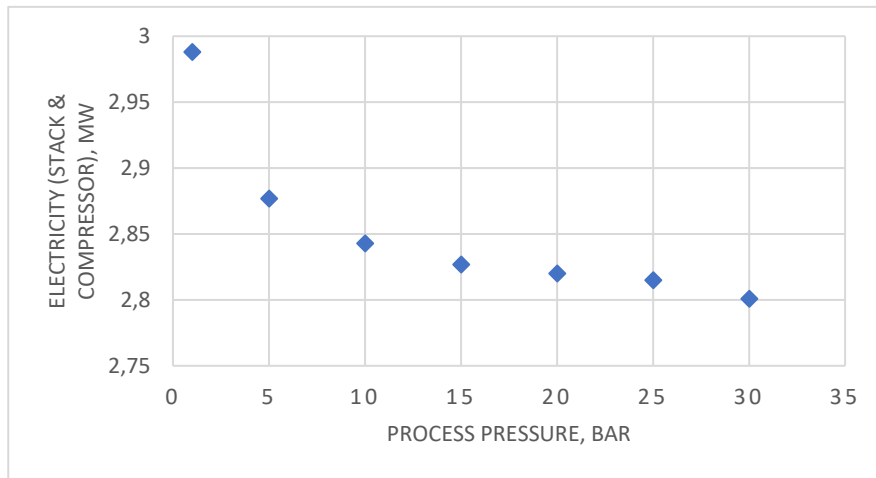
Appendix II

Table II Effect of various pressure and temperature on different process variables

Pressure, bar	Cell voltage A/cm ²					Stack power MW					H ₂ production kmol/h				
	60 °C	80 °C	100 °C	120 °C	150 °C	60 °C	80 °C	100 °C	120 °C	150 °C	60 °C	80 °C	100 °C	120 °C	150 °C
5	2.03	1.88	1.75	1.64	1.39	3.07	2.85	2.66	2.49	2.10	26.99	26.54	26.09	25.63	24.93
10	2.04	1.89	1.77	1.67	1.52	3.10	2.87	2.69	2.53	2.30	26.99	26.54	26.09	25.63	24.93
15	2.05	1.90	1.78	1.68	1.54	3.11	2.89	2.71	2.55	2.33	26.99	26.54	26.09	25.63	24.93
20	2.06	1.91	1.79	1.69	1.55	3.12	2.90	2.72	2.56	2.35	26.99	26.54	26.09	25.63	24.93
25	2.06	1.92	1.80	1.69	1.56	3.13	2.91	2.73	2.57	2.36	26.99	26.54	26.09	25.63	24.93
30	2.06	1.92	1.80	1.70	1.56	3.13	2.91	2.73	2.58	2.37	26.99	26.54	26.09	25.63	24.93
	Energy consumption kWh/kg					Stack efficiency, %					System efficiency, %				
	60 °C	80 °C	100 °C	120 °C	150 °C	60 °C	80 °C	100 °C	120 °C	150 °C	60 °C	80 °C	100 °C	120 °C	150 °C
5	56.49	53.25	50.62	48.24	41.82	70	74	78	82	94	68	72	76	79	91
10	56.91	53.74	51.19	48.98	45.84	69	73	77	80	86	68	72	75	78	83
15	57.16	54.01	51.49	49.34	46.41	69	73	77	80	85	67	71	75	78	82
20	57.34	54.20	51.71	49.59	46.74	69	73	76	79	84	67	71	74	77	82
25	57.47	54.43	51.87	49.77	46.98	69	73	76	79	84	67	71	74	77	81
30	57.58	54.47	52.00	49.92	47.16	68	72	76	79	84	67	71	74	77	81

Appendix 3

Table III Effect of various pressure on power, compressor, investment cost, and electricity cost



Appendix 4

Table IV Main equipment sizing

Equipment type	Material	Temperature, °C	Pressure, bar	Height, m	Diameter, m	Mass flow, kg/h	Flowing material in equipment	Volume, in m³
Liquid-gas separator (O ₂ -SEP)	Nickel-coated Stainless steel 316	80	16	4.72	1.52	27031.6	liquid, gas	8.62
Isothermal reactor (AE)	Nickel-coated Stainless steel 316	80	16	5.79	1.52	71439	liquid	10.56
H ₂ -O ₂ separator (B4)	Nickel-coated Stainless steel 316	80	16	4.72	1.52	71439	vapor, liquid	8.62
Liquid-vapor separator (VAP-SEP)	Nickel-coated Stainless steel 316	80	16	5.49	1.83	71439	vapor, liquid	14.41
Liquid-gas separator (H ₂ -SEP)	Nickel-coated Stainless steel 316	80	16	4.72	1.52	35477.4	liquid, gas	8.62
DEOXO reactor (DEOXO)	Nickel-coated Stainless steel 316	80	16	1	0.91	557	liquid, gas	2.40

Dryer	Nickel-coated Stainless steel 316	80	16	3.66	0.91	92.628	liquid, gas	2.40
Liquid-gas separator (SEP3)	Nickel-coated Stainless steel 316	80	16	3.66	0.91	76	gas, gas	2.40
Liquid-gas separator (SEP4)	Nickel-coated Stainless steel 316	80	16	3.66	0.91	548	gas, gas	2.40

Table V Heat exchangers.

Equipment type	Material	Temperature Hot side, °C	Temperature Cold side, °C	Pressure bar	Area m²	Hot side flow	Cold side flow
Heat exchanger (HE1)	Stainless steel 316	80	1	16	10	Liquid	Water
Heat exchanger (HE2)	Stainless steel 316	80	1	16	10	Liquid	Water
Air cooler (AIRCOOL)	Stainless steel 316	22	0	10	2.56122	Water	Water
Intercooler (COOLER)	Stainless steel 316	80	-	16	5.72353	Hydrogen	-
Intercooler (COOLER)	Stainless steel 316	107	-	30	4.64534	Hydrogen	-

Table VI Compressors and pumps

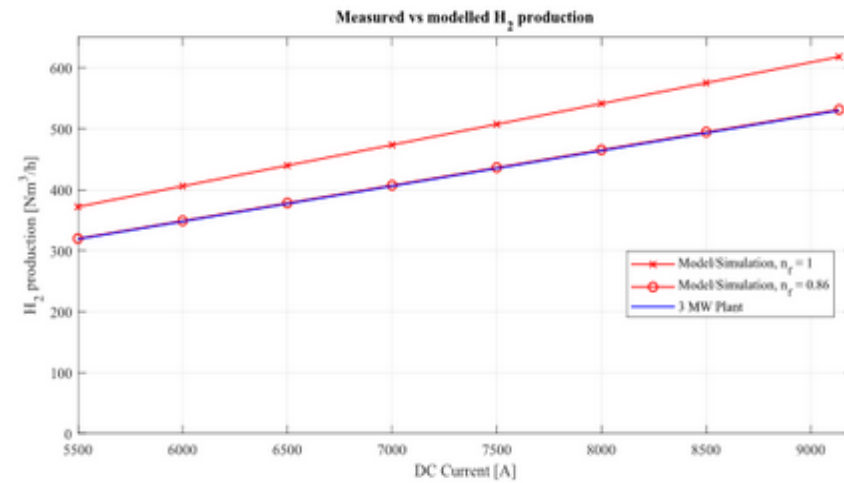
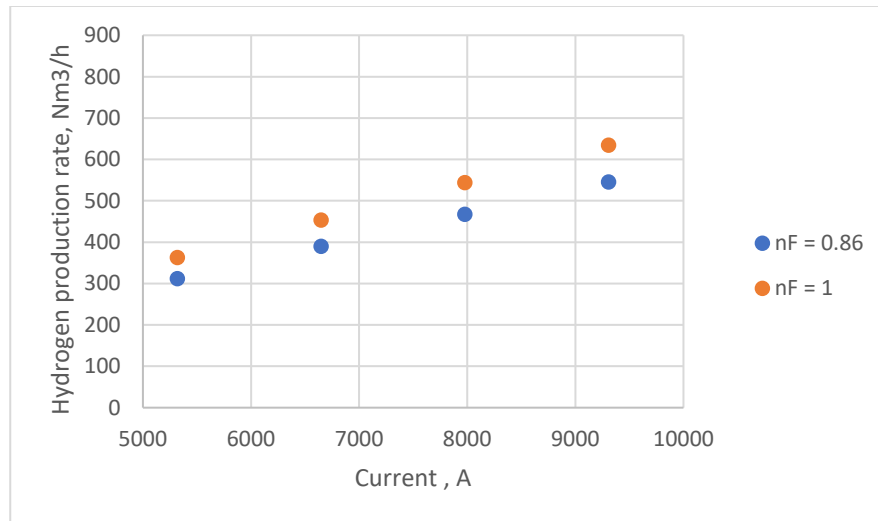
Equipment type	Material	Temperature °C	Pressure bar	Material in streams	Flow rate, m ³ /s	Theoretical power, kW	Efficiency, %	Pressure difference (bar) between targets
Compressor	Stainless steel 316	25	16	Hydrogen	0.017571	52.5629	72	14
Compressor 2	Stainless steel 316	25	30	Hydrogen	0.0079117	18.8999	72	20
Pump (pump1)	Stainless steel 316	25	1	Water	0.000263	0.92097	-	15
Pump (pump2)	Stainless steel 316	80	16	Liquid	0.012486	8.07668	-	5
Pump (pump3)	Stainless steel 316	80	16	Liquid	0.012288	7.97173	-	5
Pump (pump4)	Stainless steel 316	0	2	Water	0.000082	0.02234	-	8

Table VII Overall mass balance

Stream	Inlet						Outlet		
	H ₂ OIN	KOH	COOLH ₂ O	H ₂ -OUT	O ₂ -OUT	PURGE1	PURGE2	PURGE	CH ₂ Oout
Mass flow, kg/h	27031.600	9010.530	1000	69.486	548.048	23.909	8.556	0.326	1000
H ₂ O	1		1			1	1		1
KOH		1							
H ₂				1				1	
O ₂					1				

Appendix 4

Table VIII Calculated results compared to Sakas et al measured and modelled results.



Appendix 5

Table IX Cell voltage analysis on Matlab

```

clc;
close all;
clear all;

%%%%%%%%%%%%%%%%%%%%%%%%%%%%%%%%%%%%%%%%%%%%%%%%%%%%%%%%%%%%%%%%%%%%%%%%
%% Cell voltage analysis
%%%%%%%%%%%%%%%%%%%%%%%%%%%%%%%%%%%%%%%%%%%%%%%%%%%%%%%%%%%%%%%%%%%%%%%%

%% Variables

Urev = 1.23;           %Reversible voltage (V)
r1 = 8e-1;            %(Ohm cm^-2)
r2 = -7.63e-3;        %(Ohm cm^-2 °C^-1)
s = 0.1795;          %(V)
t1 = 20;              %(cm^2 A^-1)
t2 = 0.1;             %(cm^2 °C A^-1)
t3 = 3.5e5;           %(cm^2 °C^2 A^-1)
d1 = -3.13e-2;        %(Ohm cm^2)
d2 = 4.47e-3;         %(Ohm cm^2 bar^-1)

i = 0:0.05:0.5;       %Current density (A cm^-2)
p = 16;               %Pressure (barg)

% Define temperature range and interval_
temperature_range = 60:10:150; % Temperature range (°C)

% Initialize cell voltage matrix
Ucell_all_temps = zeros(length(i), length(temperature_range));

% Loop through each temperature
for idx = 1:length(temperature_range)
    T = temperature_range(idx); % Current temperature (°C)

    % Cell voltage calculation
    Ucell = Urev + (r1 + d1 + r2*T + d2*p)*i + s*log((t1 + t2/T + t3/T^2)*i + 1);

    % Store cell voltage for this temperature
    Ucell_all_temps(:, idx) = Ucell;
end

% Plot cell voltage for each temperature
figure('name', 'Ucell vs Temperature');
hold on;
for idx = 1:length(temperature_range)
    plot(i, Ucell_all_temps(:, idx), 'DisplayName', sprintf('T = %d°C', temperature_range(idx)));
end
hold off;
grid on;
xlabel('Current density (A cm^-2)');
ylabel('Cell voltage (V)');
legend('show');

```